Monitoring surface deformation with spaceborne radar interferometry in landslide complexes: insights from the Brienz/Brinzauls slope instability, Swiss Alps

Andrea Manconi[1,2,3*], Nina Jones[1,2], Simon Loew[1], Tazio Strozzi[2], Rafael Caduff[2], Urs Wegmueller[2]

[1] ETH Zurich, Dept. of Earth Sciences, Engineering Geology, Zurich, Switzerland

[2] GAMMA Remote Sensing AG, Gümligen, Switzerland

[3] now at CERC, WSL Institute for Snow and Avalanche Research SLF, Davos, Switzerland

*Corresponding author: andrea.manconi@slf.ch

This is a non-peer reviewed preprint that has been submitted to "Landslides"

Abstract

We performed an extensive analysis of C-Band SAR datasets provided by the European Space Agency (ESA) satellites ERS-1/2, Envisat ASAR, and Sentinel-1 in the period 1992-2020 aiming at reconstructing the multi-decadal spatial and temporal evolution of the surface displacements at the Brienz/Brinzauls landslide complex, located in canton Graubünden (Switzerland). To this end, we analyzed about 1’000 SAR images by applying differential interferometry (InSAR), multitemporal stacking, and Persistent Scatterer Interferometry (PSI) approaches. Moreover, we jointly considered Digital Image Correlation (DIC) on high resolution multi-temporal Digital Terrain Models (DTM) generated form airborne surveys and InSAR results to compute 3-D surface deformation fields. The extensive network of GNSS stations across the Brienz landslide complex allowed us to extensively validate the deformation results obtained in our remote sensing analyses. Here, we illustrate the limitations occurring when relying on InSAR and/or PSI measurements for the analysis and interpretation of complex landslide scenarios, especially in cases of relevant spatial and temporal heterogeneities of the deformation field. The joint use of InSAR and DIC can deliver a better picture of the evolution of the deformation field, however, not for all displacement components. Since InSAR, PSI and DIC measurements are nowadays routinely used in the framework of local investigations, as well as in regional, national and/or continental monitoring programs, our results are of major importance for users aiming at a comprehensive understanding of these datasets in landslide scenarios.

Keywords:

Landslide, InSAR, Monitoring, Surface deformation, Swiss Alps

1. Introduction

Remote sensing has proven in the last years to be a valid complement to standard in-situ methods for the investigation and analysis of geohazards (Tomás and Li 2017). In particular, optical and radar satellite-based imagery provided great advances in the identification, mapping, and quantification of surface changes caused by earthquakes (Jelének and Kopačková-Strnadová 2021), volcanic deformation (Ebmeier et al. 2018), land subsidence (Peng et al. 2022), and slope instabilities (Lissak et al. 2020). A prominent technique to measure surface displacements from space is the Synthetic Aperture Radar differential interferometry (InSAR). This approach relies on the identification of phase differences between multi-temporal SAR acquisitions (Bürgmann et al. 2000). The analysis of multi-temporal SAR datasets with specific algorithms (e.g., Persistent Scatterer Interferometry, PSI, or Small-Baseline Interferometry, SBAS) allows the generating of ground velocity maps and displacement time series, reaching (in ideal cases) sub-centimetric accuracies (Ferretti et al. 2001, 2011; Berardino et al. 2002; Werner et al. 2003; Hooper 2008).

PSI applications revolutionized the investigation of surface deformation associated with landslide processes (Crosetto et al. 2016). The possibility to obtain data of surface deformation at relatively high spatial and temporal resolutions without installing costly instrumentation is an essential monitoring tool to investigate and interpret landslide processes (Casagli et al. 2016). The current availability of regional, country-scale, and even continental-scale PSI datasets (Crosetto et al. 2020; Lanari et al. 2020) changed the perspective not only in research activities, but also the daily work of practitioners, as well as civil protection strategies (Dehls et al. 2019; Raspini et al. 2019; Bianchini et al. 2021). Intrinsic limitations, however, might hinder the nominal performance of InSAR and PSI in mountain areas (Wasowski and Bovenga 2014; Manconi et al. 2018). For example the presence of vegetation and/or snow cover, as well as steep areas affected by geometric distortions in radar geometry cannot be efficiently monitored (Cigna et al. 2014). Additionally, InSAR measurements are in one dimension only, i.e., along the satellite's line of sight (LOS), and a combination of a minimum of two or more satellite orbits is required to extract displacement in two and three dimensions (Delbridge et al. 2016; Li et al. 2019). Due to typically nearly-polar orbits of SAR satellites, however, slope movement along the satellite's track (i.e., almost in North-South directions) remains unmeasured or severely underestimated (Wasowski and Bovenga 2014). Atmospheric phase screen may also seriously affect the accuracy of measurements if not properly considered and corrected (Dini et al. 2019).

Another important limitation of InSAR is that accurate measurements are prevented when the surface deformation is relatively large, rapid, and/or spatially and temporally heterogeneous (Manconi 2021). This can be of particular importance when analyzing large landslide complexes, which may have a heterogeneous evolution characterized by non-steady velocities, development of different compartments, and generate potentially local failure events (Stead and Eberhardt 2013; Agliardi et al. 2020). Large and/or rapid displacements can still be measured from SAR images with other approaches, as for example the Digital Image Correlation method (DIC, known also as pixel-offset, speckle- or feature-tracking). This is an efficient workaround to retrieve measurements also where large spatial gradients occur; however, the accuracy of the measurements is related to the ground sampling distance (GSD) of the imagery used, which in the case of SAR satellites is typically on the order of meters (Casu et al. 2011; Manconi et al. 2014). Some authors have shown how joint analysis and integration of standard InSAR, DIC, and PSI can be used to investigate large compound landslides, although such comprehensive studies are unusual (Singleton et al. 2014; Li et al. 2019).

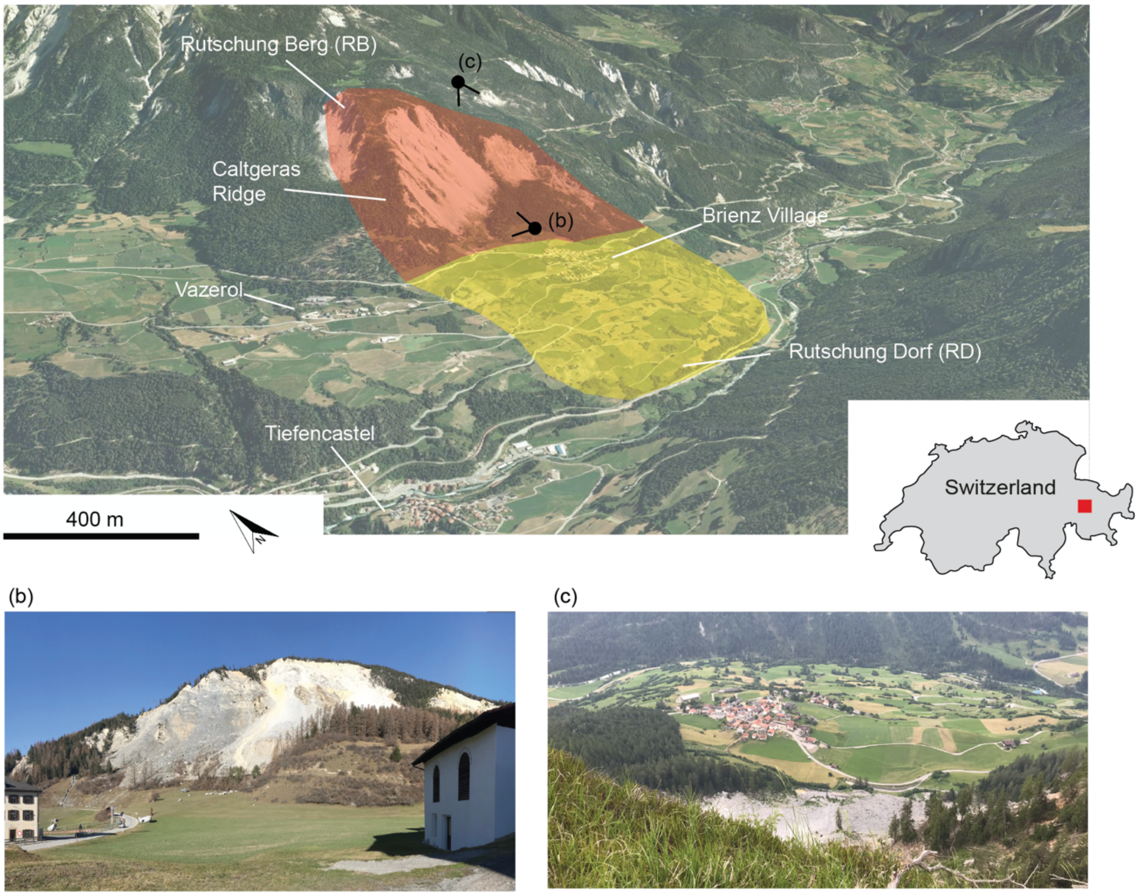

***Figure 1**: (top) Overview of the Brienz landslide complex (location shown in the inset), background Google Earth imagery. The main morphological distinctions are identified in red (Rutschung Berg, RB) and yellow (Rutschung Dorf, RD), respectively. Two exemplary pictures are shown to highlight the morphological differences between the higher and the lower portions of the slope affected by surface deformation (picture locations and fields of view are shown in the top panel in black).*

Here we present an extensive analysis of C-Band SAR datasets (frequency 5.4 GHz, wavelength ca. 5.6 cm) acquired from the European Space Agency (ESA) radar missions, i.e., ERS-1/2, Envisat ASAR, and Sentinel-1, covering the period 1992-2020. We reconstruct the spatial and temporal evolution of the surface displacements over ca. 30 years at the Brienz/Brinzauls landslide complex (hereafter referred to as Brienz, see Figure 1), located in canton Graubünden (Switzerland). We compare our results against ground-based GNSS measurements and independent information derived from additional radar sensors (Radarsat-2 and ALOS-2 PALSAR-2). To complement the InSAR analysis, we also considered DIC on multi-temporal Digital Terrain Models (DTM) generated form airborne LiDAR surveys. The latter were combined with InSAR results to compute the 3-D surface deformation field.

We completed our analysis up to 2020, i.e. before a further dramatic increase in landslide velocity led to the evacuation of the village of Brienz at the beginning of May 2023, culminating with a failure event on June 15, 2023, with a mass wasting of about 1.2 Mm^3 (Loew et al., 2023). We deliberately focus on the analysis of the long-term evolution of surface displacements occurring before this major event. The time frame before the event (2020-2023) and additional details on the catastrophic failure are not covered here and will be the subject of future publications, for which specific analyses are presently carried out. The aim of this work is manifold. We target at showing and discussing how spatial and temporal heterogeneities might strongly influence the investigation of displacements in complex landslide scenarios when relying on C-Band InSAR satellite measurements only. In most cases only little or no constraints from field data is available; thus, our results in one of the best monitored landslides in the Alps provide important assessments on accuracy and challenges of such analyses in complex scenarios in other regions. In addition, we show how a careful use of InSAR based results, not only on PSI but also on wrapped, unwrapped, and stacked interferograms, can be of great value, but often not sufficient to fully judge spatial and temporal heterogeneities.

2. Background on the study area

The Brienz Mountain slope deformation, located in canton Graubünden, Switzerland, affects a large portion of the southern flank of Piz Linard and the Albula river, and includes the village of Brienz/Brinzauls (765'048 E, 1'170'830 N, CH1903/LV03). The active parts of this mountain slope deformation occur the lower slope areas (below about 1800 m a.s.l and form a very heterogeneous landslide complex. The geomorphological, hydrogeological, and subsurface geological conditions of the active part of this landslide complex have been investigated in detail during the last years (Figi et al., 2022). The currently active upper slope portions (namely the “Rutschung Berg”, i.e., expression to indicate “Landslide affecting the mountain” in German language, hereafter referred to as RB) are located between approximately 1’770 m and 1’150 m a.s.l., with an average slope of 36 degrees. The currently active lower slope portions (namely “Rutschung Dorf”, i.e., expression to indicate the “Landslide affecting the village” in German language, hereafter referred to as RD) extend from about 1’150 m a.s.l. to the Albula riverbed located at approx. 870 m a.s.l, with an average slope of 8 degrees. The landslide involves low-grade sedimentary units of the Penninic and Austroalpine nappes with strong differences in mechanical properties. In particular, the RB and RB domains include (from bottom up) located in North Penninic Flysch units, South Penninic Allgäu Schists, Austroalpine Arlberg Dolomite and Raibler Schists units. The Brienz landslide complex is composed of a series of stacked old rockslides, rock mass fall deposits and dry/moist granular flows. In the frontal 400-500 m the RD have been thrusted over Late-glacial and Holocene fluvial deposits of the Albula river. Remarkable morphological and geological heterogeneities in RB lead to a distinction into different landslide compartments having different surface velocity amplitudes and directions, as well as different kinematic and dynamic behaviors. In Figure 2, we show the approximate delimitation and naming of the main landslide compartments. A full description of the characteristics of the is beyond the scope of this paper. Details on the geological, structural setting, hydrogeology and dynamic behavior can be found in (Figi et al. 2022).

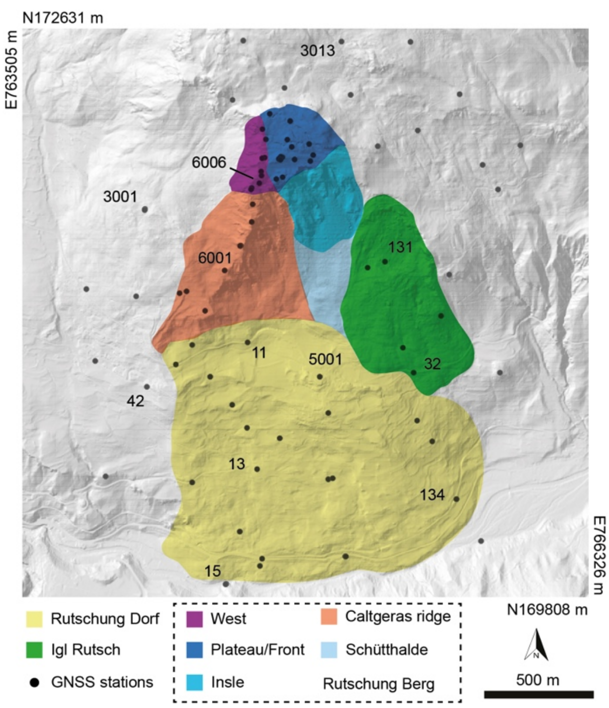

***Figure 2**: Approximate delimitation and naming of the active compartments (cf. Figi et al., 2022). Black dots show the location of GNSS stations (full set with coordinates reported in the Supplementary Information, Table S1). Shaded relief generated from the SwissALTI3D digital model (source, swisstopo, 2013, GSD 2 m).*

Large surface displacements and catastrophic failure potential cause major concerns to the authorities because approx. 100 people permanently reside in the Brienz village, with up to 200 people during holiday periods. In addition, several important connecting roads and a railway line are affected by damages. Slope instability and rock falls have been a recurrent problem for the Brienz population. In the eastern side of the slope, a large earthflow (known as "Igl Rutsch") accelerated in November 1878, and reached velocities of up to 1 m/day, alarming the inhabitants for several months before resting (Ludwig, 2011). Since 1921 the displacements on the village have been periodically measured, and in 2011 a permanent total station was installed to continuously monitor target points in RB and RD. Average surface velocities increased in the entire slope since 2015, and for this reason, the monitoring network has been expanded. This includes a combination of periodic surveys and permanent GNSS stations with currently more than 80 points, as well as more than 40 reflectors. Moreover, surface displacements are also continuously monitored with a permanent ground-based SAR, and the network is complemented with time lapse cameras acquiring multi-temporal pictures form different locations, as well as with a doppler radar system aimed at detecting rock falls potentially reaching the road connecting Brienz to Vazerol (Schneider et al. 2023). In addition, the dynamic response of the landslide is monitored by analyzing ambient vibration recorded through a network of broadband seismometers (Häusler et al. 2022). All these data have been extremely important for the implementation of an early warning system, which allowed to recognize timely the critical slope acceleration in spring 2023 and the subsequent evacuation of the population before the slope failure event (Loew et al., 2023).

3. Surface deformation from remote sensing

In this work, we considered multiple datasets and methodologies, including:

(1) Differential interferograms considering all available ESA C-Band satellite imagery (993 images in total, see details in Table 2) acquired from ascending and descending orbits of ERS-1/2 (1992-2000), Envisat ASAR (2004-2010), and Sentinel-1 (2015-2020). The InSAR analysis is performed to obtain initial surface velocity maps by considering different time intervals and served to potentially identify the initiation and the variability of surface displacement in the different domains of the Brienz slope, as well as possibly their main periods of activity. Moreover, we stacked selected Sentinel-1 interferograms from three different orbits, one ascending and two descending. This approach has been used to increase the signal-to-noise ratio, mitigate atmospheric disturbances, and to provide averaged, spatially continuous surface velocity maps over the entire Brienz slope.

Satellite	Orbits (# images)	Period available	Revisit time (days)
ERS-1/2	T215A (#38) T480D (#65)	1992-2000	35
Envisat ASAR	T215A (#37) T480D (#42)	2004-2010	35
Sentinel-1	T015A (#258) T066D (#275) T168D (#278)	2015-2020	6*

Table 2. Summary table of the ESA C-band SAR dataset available. The A in the orbit name stands for ascending tracks, while D for descending. *The Sentinel-1 revisit time of 6 days is available after 2017. Before this date the revisit time is 12 days.

(2) Persistent Scatterer Interferometry (PSI) on data acquired from ERS-1/2, Envisat ASAR, and Sentinel-1, each on ascending and descending orbit. We considered the Interferometric Point Target Analysis (IPTA, Werner et al., 2003), aiming at computing surface velocity maps and displacement time series at point targets maintaining a good coherence (i.e., SAR signal quality).

(3) Digital Image Correlation (DIC) applied to four Digital Terrain Models (DTMs) generated from airborne LiDAR. The data were acquired by helicopter on November 12, 2015, June 15, 2018, December 6, 2019, and September 4, 2020, respectively. The DIC analysis provided measurements over areas affected by large displacements, i.e., where DInSAR usually fails to provide useful results.

(4) 3-D surface displacements for two selected periods, i.e., 2015-2018 and 2018-2020. Sentinel-1 stacking computed in (1) and the DIC results obtained in (3) have been jointly used to obtain a full description of the displacement field, as well as hints on the temporal evolution of the landslide complex.

To ease following our workflow and the reading, in the sections below we sequentially describe the methods and directly present the most relevant results. Additional outcomes (in particular, selected wrapped interferograms) are reported in the Supplementary Information (see Figures S1-S8) and discussed in section 5.

3.1. Differential interferometry and multitemporal stacking.

We computed surface displacement maps with differential interferometry by considering pairs of SAR images after alignment (also known as co-registration) and removal of the phase contribution due to topography (Bürgmann et al. 2000). The products obtained (i.e., differential interferograms) were visually inspected in their wrapped phase form, and then unwrapped by considering the MCF algorithm (Costantini 1998). For each satellite and orbit, we stacked selected interferograms with good quality (i.e., spatial coherence). Stacking methodologies are frequently used in geophysical data processing and remote sensing analyses in order to improve the signal-to-noise ratio (Stumpf et al. 2017; Gorelick et al. 2017). Regarding InSAR, stacking is generally performed by combining multiple unwrapped differential interferograms covering a pre-defined time period (e.g., one or multiple years), in order to highlight spatial domains retaining surface velocities within this time frame (Lundgren et al. 2001; Ciuffi et al. 2021). Any artefacts affecting single acquisitions are expected to have random variability over time and thus be mitigated with integration and/or averaging of the signal, provided that enough input images are available.

3.1.1 Results

No clear signs of surface displacements are evident in the period 1992-2010 with standard InSAR analyses on ERS-1/2 and Envisat ASAR (see also Supplementary Information S1-S2), although during this period minor surface activity was already known and measurable in-situ. Single interferograms considering temporal baselines ranging from 35 days to one year were not successful in retrieving suitable measurements due to the excessive noise levels. Failure to retrieve measurements can be explained mainly due to relatively poor quality (in terms of spatial and temporal baselines) of the data available in this time range in comparison to the rates of motion and landcover. Figure 3 shows the results of annual stacking obtained for the Sentinel-1 orbits, which provide the most valuable results when selecting interferograms with perpendicular baselines (orbit separations) below 150 m and temporal baselines as short as 12 days. Interferograms with longer temporal baselines suffer from a substantial drop in coherence and were not beneficial in our investigation.

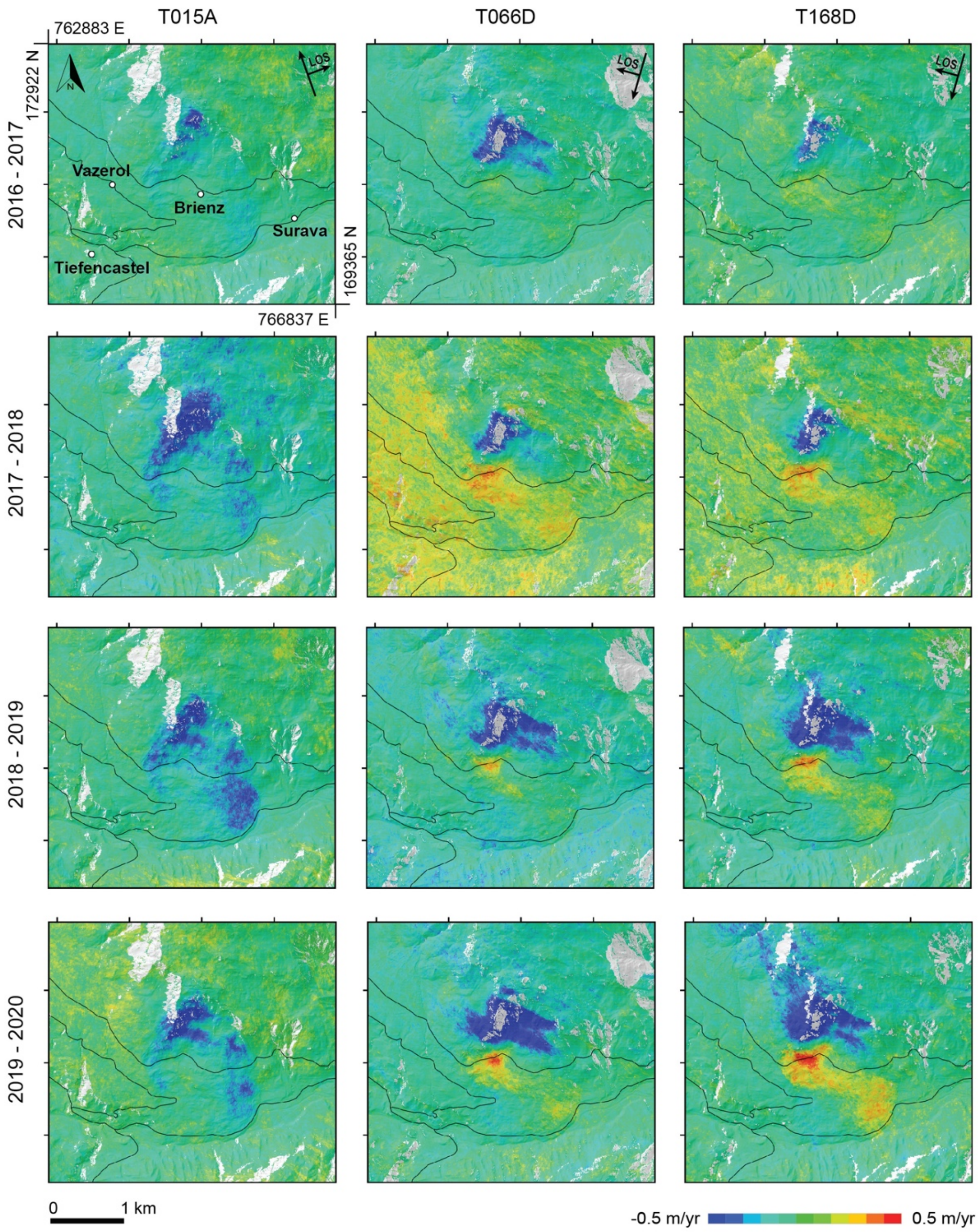

Figure 3: Results of the annual Sentinel-1 stacking analysis. Velocities are in satellite LOS. Negative values (blue) mean that the ground moved away from the satellite, while positive values (red) indicate that the ground moved towards the satellite. Black solid lines represent the main connection roads and are shown in all tiles to provide a spatial reference. Missing results are due to layover/shadow masking.

Sentinel stacks were generated considering the same observation periods for each orbit, consistently starting in the beginning of September of each year, highlighting inter-annual variability. We set coherence thresholds aiming at increasing the quality of the final stacking products, however, no significant improvement was observed and thus we decided to present the results here without thresholding. We attempted shorter stacking, covering about three months to potentially identify intra-annual and/or seasonal variabilities, but results were inconclusive. We also tried stacking solely Sentinel-1 interferograms with temporal baselines of 6 days, but this approach drastically reduced the number of input images, compromising the effectiveness of the procedure.

A striking observation are the remarkable differences in the spatial distribution of the displacement signal when comparing ascending and the two descending results. Results of T015A highlight mainly LOS movement away from the satellite in RB and the outer extents of RD in a "horseshoe-like" pattern. Distinct signals showing a different LOS sign for RB and RD are instead detected in descending orbits, where the surface displacements change sign even within the RD domain at the landslide toe, in the area close to the Albula river. This spatial variability suggests a strong heterogeneity of the surface displacements directions, combined with the remarkable topographic variations of the area under investigation. Focusing on the temporal behavior, a progressive increase of the surface displacements can be observed at selected locations, although this is not very clear in all considered orbits (Figure 4). For example, surface velocities at the Brienz village appear to be very small in the period 2016-2017 compared with the portions of RB located at higher elevations. After 2017, the RD displacement pattern starts to be more evident and locally of the same order of magnitude as RB. The upper extent of RB also shows a remarkable increase in surface velocities over the analyzed time. Near the GNSS stations 6006 and 6001 (see locations in Figure 2), LOS surface velocities were of about 0.2-0.4 m/a in the period 2016-2018 but reached values up to 1 m/a in 2019-2020. Moreover, eastern portion of the instability shows a remarkable acceleration from 0.2 m/a in 2016-2017 to about 0.3-0.4 m/a in 2018-2020. Some discrepancies between the results obtained by different orbits can be related to the changes in viewing angles and/or to random noise on the stacking products. Considering the variability of the results in the vicinity of areas assumed stable over the analyzed period, for example near GNSS point 42 located in the village of Vazerol, the expected level of accuracy of the stacking results is on the order of 0.1 m/a. This value is higher in areas where the displacements are of several m/a.

3.2 Interferometric Point Target Analysis (IPTA)

PSI is considered an advanced remote sensing method; however, in the last few years this approach has gained more and more popularity and can be considered as a standard approach for the investigation of surface displacements on unstable slopes (Wasowski and Bovenga 2014). This is mainly due to the availability of new generation satellites such as the ESA Sentinel-1 constellation, which provides reliable acquisitions at global scales and with unprecedented spatial and temporal resolutions (Torres et al. 2012).

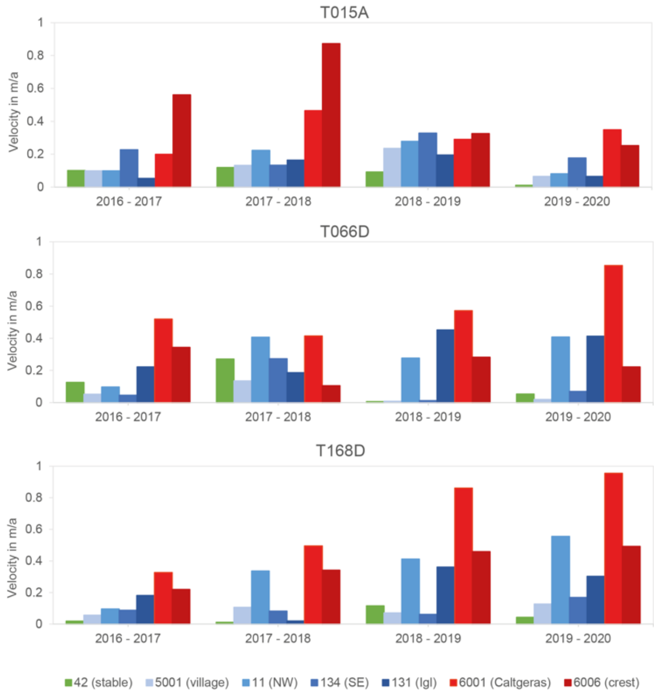

***Figure 4**: Results of the annual stacking at selected locations (see Figure 2 for the position of points). Velocities are in satellite LOS.*

Several projects have been developed to provide wide-area coverage of PSI results (Zinno et al. 2018; Dehls et al. 2019; Crosetto et al. 2020), which directly provide to the end-users PSI results in the form of surface velocity maps and displacement time series. Here we performed PSI processing on two relevant Sentinel-1 tracks, by applying the IPTA method on "single-reference" stacks (GAMMA Software, Wegmüller et al., 2016). This is one of the most diffused approaches for multi-temporal DInSAR analyses over unstable slope regions. The reference images for the IPTA processing were selected in the middle of the entire time of analysis (about five years), i.e., July 23, 2018, and July 27, 2018, for T015A and T066D, respectively. This choice helped to balance the temporal baselines of the processed pairs and expected to improve interferometric coherence. Due to the accurate control of the Sentinel-1 orbital parameters, the spatial baseline between all acquisitions and the reference image is generally below 150 m, ensuring a good quality of the SAR phase and thus more reliable displacement measurements.

3.2.1 Results

Figure 5 shows the Sentinel-1 surface velocities over the Brienz slope complex achieved with IPTA processing, compared with previous results obtained by considering ERS and Envisat ASAR sensors in the ESA GMES TERRAFIRMA project (Raetzo et al. 2007), for ascending and descending orbits. The relatively poor spatial coverage of point measurements is as expected. Some signs of surface displacements on the order of 0.01 cm/a can be seen in the village of Brienz starting from the period 2002-2010 (Figure 5c), however, as already evidenced in the standard InSAR and stacking analyses, the surface deformation starts to be relevant only when considering the Sentinel-1 results. The measurement points are located mainly at buildings and/or other anthropic infrastructures, as well as some rock faces maintaining a relatively good temporal coherence over the period of analysis. While no information is generally available from the IPTA on the RB portions, measurement points located at the Brienz village appear to move towards the satellite LOS in descending orbit and away from the satellite LOS in ascending orbit. This suggests that a relevant component of the surface displacement affecting the Brienz village is slope parallel and/or sub-horizontal. In the Sentionel-1 results (Figure 5e-f), some isolated points can be seen southwest of Brienz village that show an opposite sign of surface velocity. This suggests the presence of local areas with different displacement directions; however, the overall number of IPTA points is too small to perform a comprehensive interpretation. Snow cover in winter periods and rapid seasonal changes deeply affect the phase correlation in alpine regions (Wasowski and Bovenga, 2014). This cannot be avoided despite performing local investigations on the slope of interest, and thus, with all processing parameters calibrated to obtain the best solution over the study area. The time series mostly show a linear displacement trend, with some minor oscillations that might be related to seasonal variations and/or uncompensated atmospheric artefacts (see Supplementary Information, Figure S9). The ground-based measurements from 2015-2020 a substantial acceleration in the same time period (Figi et al. 2022). Discrepancies between IPTA results and in-situ observations are likely caused by the large and rapid displacements occurring over the Brienz slope complex (Manconi 2021).

3.3. Digital Image Correlation analysis

Digital Image Correlation (DIC) is a method allowing to track displacements by comparing pixel groups in multi-temporal digital imagery acquired from different sensors, mainly optical and radar, and from different platforms (ground-based, airborne, and/or spaceborne). The DIC strategy has been initially adopted on remote sensing datasets to study rapid flow of glaciers (Strozzi et al. 2002; Kääb et al. 2009). More and more often, however, this technique is used for the investigation of slope instabilities and landslide events, despite a reduced accuracy compared to standard InSAR approaches (Manconi et al. 2014). The theoretical accuracy of slope displacements measured by DIC strongly depends on the signal-to-noise ratio of the imagery, as well as on the GSD of the input data (Bickel et al., 2018; Bontemps et al., 2018; Stumpf et al., 2017). For this reason, Sentinel-1 imagery (with GSD of about 3 m in range and 15 m in azimuth direction) is often not suitable to obtain the desired accuracy levels at the slope scale.

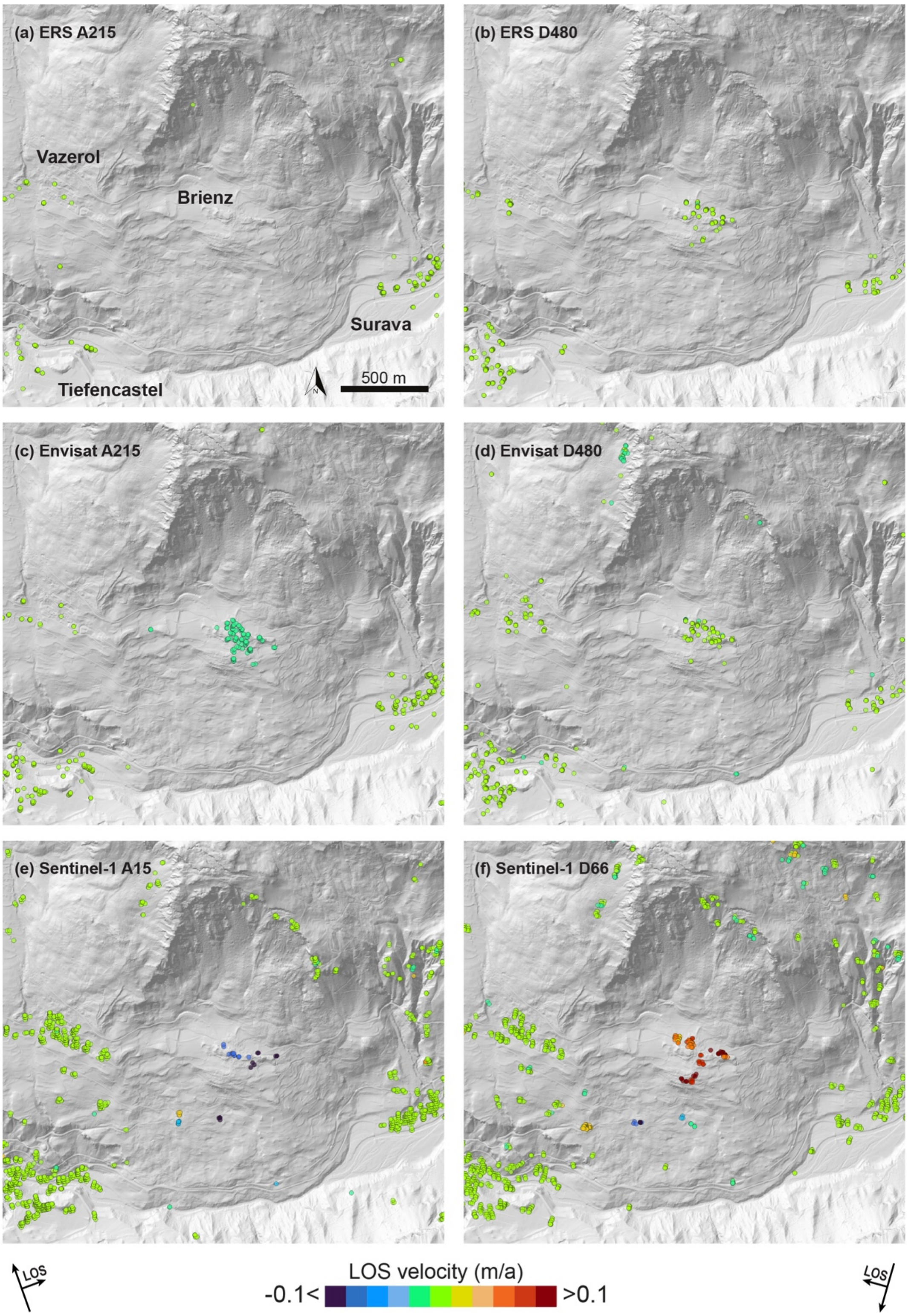

***Figure 5**: Surface velocity map over the Brienz slope obtained by applying the IPTA approach on different C-Band satellite sensors. Positive values (red) mean that the ground moved towards the satellite LOS, while negative values (blue) indicate that the ground moved away from the satellite LOS. (a) ERS ascending, 1992-2000, note the poor spatial coverage due to reduced amount of imagery in comparison with the descending orbit; (b) ERS descending, 1992-2000; (c) Envisat ASAR ascending, 2002-2010; (d) Envisat ASAR descending, 2002-2010; (e) Sentinel-1 ascending, 2015-2020; (f) Sentinel-1 descending, 2015-2020. Selected Sentinel-1 PS time series are presented in the Supplementary Information, Figure S9.*

Here we considered multi-temporal DTMs generated from airborne LiDAR surveys over the Brienz slope in the period between 2015 and 2020. First, we resampled the input data to a common grid of 1 m, as they initially entailed different GSDs. Then, we generated shaded relief images from the DTMs by considering multi-directional sun azimuth and elevation (Fey et al. 2015). The shaded relief data is projected coordinates in map coordinates (CH1903, EPSG 21781), thus, DIC results provide measurements of the displacement components occurring in the North-South and East-West directions. The DIC processing was performed using the software presented in (Bickel et al. 2018), which has already demonstrated good performances for large slope deformation related to other alpine mass movements (Manconi et al. 2018; Glueer et al. 2019; Storni et al. 2020; Aaron et al. 2021). We have done several tests to identify the parameters providing reliable results. The final DIC parameters used in this analysis are reported in the Supplementary Information, Table S2.

3.3.1 Results

DIC results are presented for two selected time windows considered important for the interpretation of the spatial and temporal evolution of the Brienz slope complex. The periods range between November 12, 2015, and June 15, 2018 (period 1), and between June 15, 2018, and September 4, 2020 (period 2). These time windows have similar durations (2.6 vs. 2.2 years) and are characterized by the transition from slow to moderate surface velocities (i.e., period 1) and then a period of sustained high velocities (i.e., period 2). The results (Figure S10) show the dominating displacement direction towards South, with velocity values exceeding 2 m/a especially in the upper RB portions as well as along the western extents of RB. The East-West displacement component is lower in magnitude, and for this reason the DIC results include more noise. Another important observation from the DIC results is that the spatial distribution of the surface displacements is very similar in the two considered periods, however, an overall increase in surface velocities is noted in the 2018-2020 period, indicating an acceleration compared to the 2015-2018 period. This agrees with the ground-based observations. One of the main issues in the DIC processing was related to boundary effects associated with poor coverage of the DTMs around the Brienz slope, i.e., in areas expected to have minor or no displacements and that can be used for the evaluation of the DIC accuracy.

3.4. Reconstruction of 3-D displacements field

Due to the increased data availability, the integration of InSAR results from multiple satellite orbits, as well as with DIC products, is increasingly popular in the analysis of slope deformation.

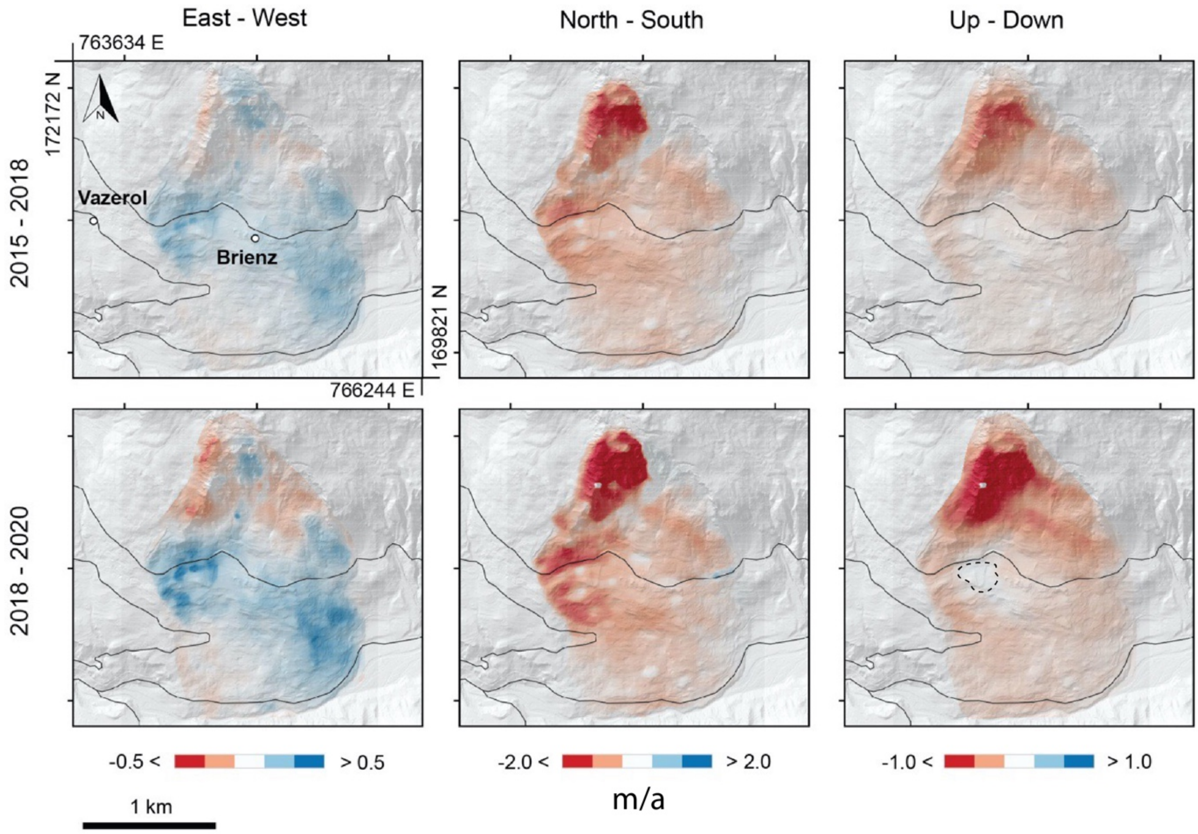

***Figure 6**. 3-D surface velocities in m/a over the Brienz landslide complex, obtained by combining the Sentinel-1 stacking and the DIC results on the LiDAR DTMs. The black dashed polygon shows the area where minor uplift has been identified (see text for more details).*

Using this approach it is possible to derive a 2-D and/or 3-D representations of the displacement field and better study the kinematic behavior of landslides (Elefante et al. 2014; Delbridge et al. 2016; Frattini et al. 2018; Crippa et al. 2020). In the specific case of Brienz, a straightforward application of the classical approach combining the Sentinel-1 ascending and descending orbits does not provide substantial benefits. The main reason is that the SAR satellites fly on a near-polar orbit (~11 degrees from North), and thus all surface displacements oriented along the satellite's track are not measurable because they produce only very small (if any) changes in the LOS. Indeed, the displacement components that can be retrieved from two or more orbits are 2-D, i.e. the vertical and East-West directions, assuming that the North-South component is negligible (Manzo et al. 2006). From the DIC results, as well as from the ground-based monitoring, we know that in Brienz the displacement amplitudes show relevant spatial variations, and that the main component of slope movement is oriented towards South. To reconstruct the 3-D displacement components, an integration of all the available results is necessary. We computed the 3-D deformation considering a least-squares estimation of the displacement components starting from multiple observations. The least-squares solution is constructed as an over-determined set of linear equations, with the design matrix solved into the Singular Value Decomposition (see for example (Casu and Manconi 2016). We exploited in total five observations (three LOS measurements from the Sentinel-1 orbits and two DIC results, in North-South and East-West directions, respectively). To this end, we have resampled the input datasets to a common grid (5x5 meters) and computed stacking products to align the temporal observation of the Sentinel-1 data with the LiDAR surveys. The calculation was thus done on the two reference periods 2015-2018 and 2018-2020.

3.4.1 Results

Figure 6 shows the 3-D surface velocities for the time periods 2015-2018 and 2018-2020. The results confirm the dominance of the South-oriented motion component. The increase of surface velocity in the period 2015-2018 can be recognized in all components, however, the changes are more remarkable in the North-South and Up-Down directions, where the velocity locally exceeds 2 m/a in RB. Uplift of few cm/a was identified West of the Brienz village, with an increasing trend in the 2018-2020 period (~6 cm/a) compared to 2015-2018 (~2 cm/a). Unfortunately, no monitoring points were installed in this area during the period of observation, thus we could not compare these results with external data. Additional GNSS survey and levelling measurements were started in summer 2021 to better understand the behavior of this zone. The source of this uplift is not clear with the information currently available.

4. Comparison with GNSS measurements

The reliability and accuracy of the surface deformation obtained with the combination of InSAR and DIC analyses has been validated with the available GNSS in-situ measurements. The extensive network of stations across the Brienz landslide complex allows for validation of the deformation results obtained in remote sensing analyses. We extracted the surface velocities for each direction at the location of GNSS stations and compared them with the velocities recorded by GNSS over the same time periods. We considered that GNSS station 42 is our stable reference (see location in Figure 2). Figure 7 shows the scatterplots comparing the stacking results obtained for the three different Sentinel-1 orbits with the GNSS measurements projected along the satellite LOS. The agreement is better in the 2015-2018 period, when surface velocities were relatively lower than during 2018-2020. However, the inaccuracy of the InSAR measurements increases as the surface velocity overcomes the temporal phase aliasing thresholds at 0.85 m/a, considering 6-days revisit time (0.425 m/a with 12-days revisit time). This is more pronounced for the points located in the RB and leads to an underestimation of surface velocities up to several m/a in comparison with GNSS measurements.

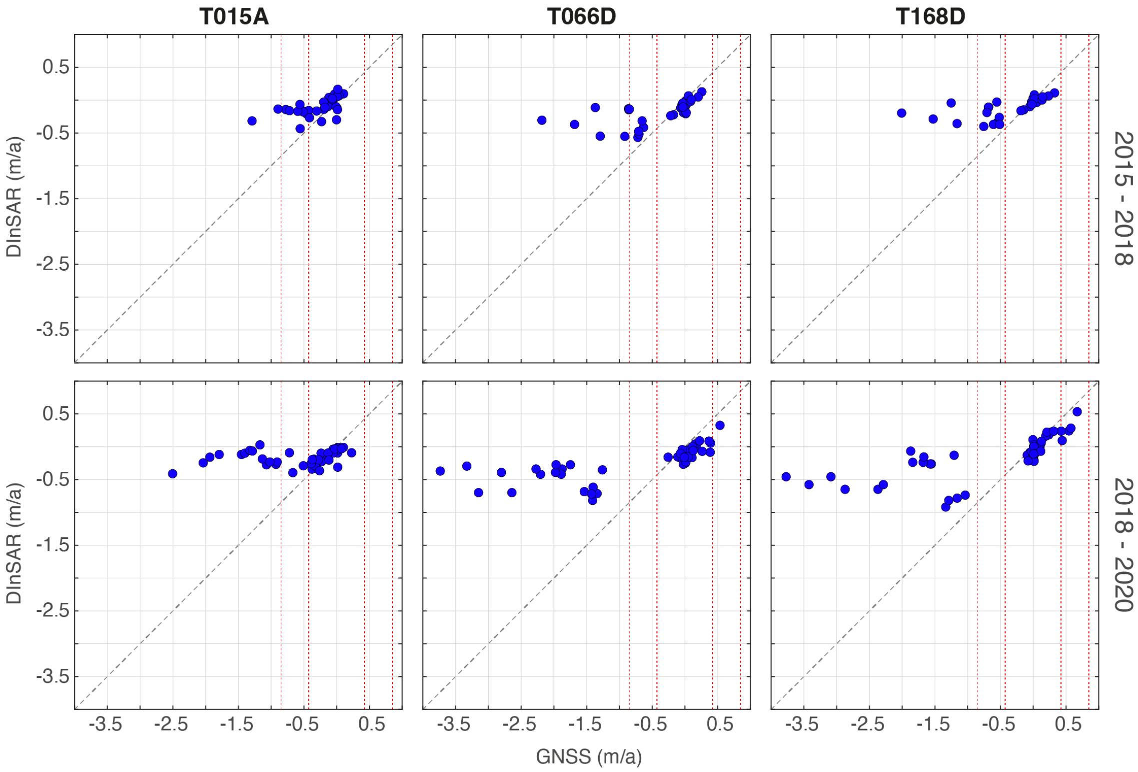

***Figure 7**. Scatterplots comparing surface velocities measured with Sentinel-1 InSAR stacking and in-situ GNSS (projected along satellite LOS). Perfect agreement is indicated when points lie on the plots' diagonal. Red dashed lines show the theoretical phase aliasing limits for 6 and 12 days (see Manconi, 2021).*

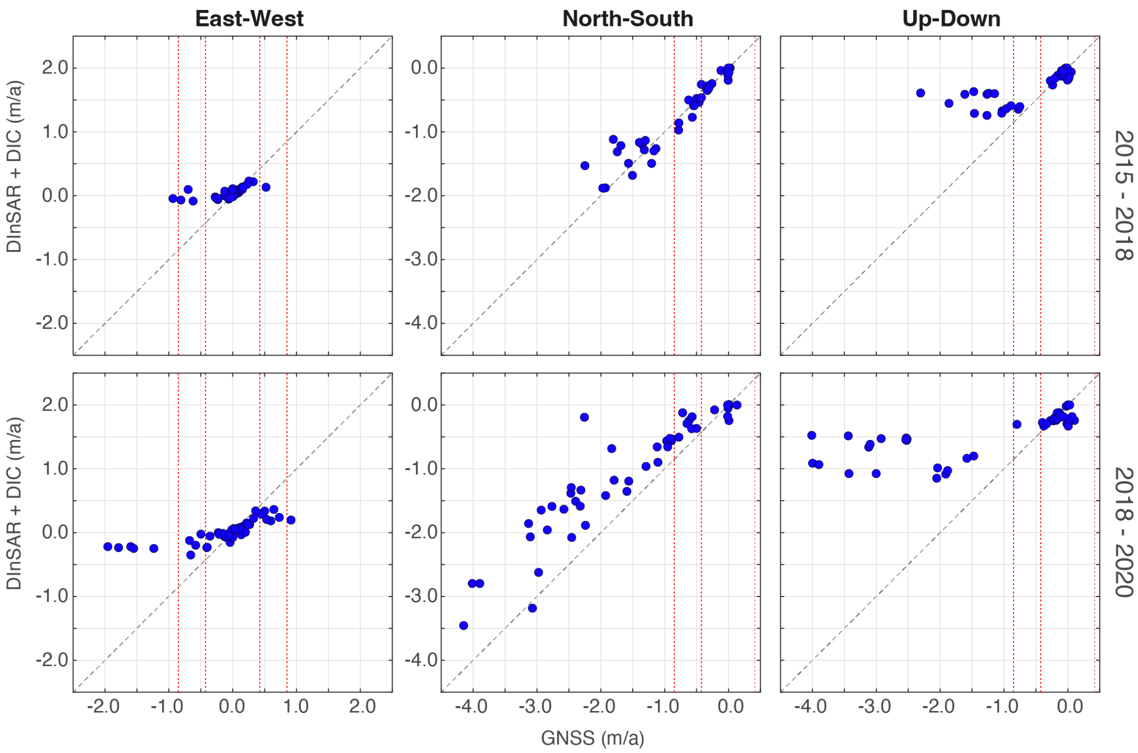

***Figure 8**. Scatterplots comparing 3-D surface velocities obtained with the combination of Sentinel-1 InSAR stacking and DIC versus in-situ GNSS. Perfect agreement is indicated when points lie on the plots' diagonal. Red dashed lines show the theoretical phase aliasing limits (see Manconi, 2021).*

Figure 8 shows the comparison of GNSS with the 3-D surface velocities obtained by combining the Sentinel-1 stacking and the DIC results. The agreement improves compared to the results of the InSAR stacking only, however, large discrepancies can still be observed. This is more evident in the vertical components, as the DIC results do not contribute to the least squares solution, and in the East-West components, as motion in these directions is relatively small compared to the North-South component and mostly below the DIC detection thresholds (see also Supplementary Information, Figure S10). In general, the main discrepancies with the GNSS measurements are related to the underestimation of the vertical component in the upper portions of the RB. The North-South component gains better agreement to the GNSS measurements; however, in the 2018-2020 period there is still a clear underestimation of the surface velocities.

6. Discussion and conclusions

The results attained with extensive investigations of remote sensing datasets can be of great value for the evaluation of the state of activity of landslide complexes. However, we have shown that several problems can be encountered. The main difficulties arise during processing of the critical stage from slow to fast surface displacement observed at large deep-seated slope instabilities (Agliardi et al. 2020). This period can last for several years or rapidly evolve on the order of few weeks and potentially increase the probability of catastrophic slope failures.

We provide numerous indications of the spatial and temporal evolution of surface displacement occurring at the Brienz slope complex in the period 1992-2020, ca. 30 years. First, we revealed that PSI analyses over heterogeneous, complex landslide scenarios such as Brienz, affected by large and/or rapid surface velocities, are not suitable for a comprehensive investigation of the spatial and temporal kinematic evolution. The main problems are related to the reduced coherence of the SAR phase, which leads to inaccurate displacement measurements and poor PS spatial coverage. The analysis of selected Sentinel-1 interferograms indicates that the RB domain in the period 2015-2018 has constant high levels of surface displacements, which can hardly be accurately detected with InSAR of image pairs acquired more than 18 days apart due to phase decorrelation. By stacking Sentinel-1 interferograms, it has been possible to reconstruct at least the yearly trends of surface displacements on one ascending and two descending orbits. These results provide a fair overview of the spatial distribution of surface deformation over the last five years, as well as information on their temporal evolution. In the RB domain the displacement amplitudes have increased between 2015 and 2020, while the

RD domain shows an overall similar displacement behavior throughout the analyzed period. The only area with a relevant increase in surface displacement within this time frame is located to the West of the Brienz village.

We have also used additional satellite sensors to cross-validate the InSAR results. The analysis of the Radarsat-2 dataset has provided suitable results for a limited number of interferograms covering the period 2014-2019 despite the very-high spatial resolution of 5 m (see also Supplementary Information S3-S4). Moreover, the information is available only for summer periods. This period is already covered by the Sentinel-1 imagery, which has a more frequent revisit time compared to Radarsat-2 (6 to 12 days vs. 24 days) and thus provided better results (see also Supplementary Information S5-S7). ALOS-2 PALSAR-2 satellite data (L-band SAR imagery) for selected dates can retrieve more deformation than C-band in the RB area (see also Supplementary Information S8). Due to its longer wavelength (ca. 23 cm), L-band is less impacted by phase decorrelation caused by large movement and potentially local failure, and/or can follow displacements occurring in areas with vegetation (Aoki et al. 2021). Additional indications are provided on the surface deformation affecting the areas are not covered by GNSS or total station monitoring (eastern slope portions). Unfortunately, the L-band data were very limited over our area of interest. Additional datasets acquired from SAOCOM, as well as future satellite missions planned with L-band SAR such as the NISAR, ALOS-3 PALSAR-4 and ROSE-L, will be an important source of information for landslide analyses in complex scenarios such as the Brienz case (Rosen et al. 2017).

Due to the intrinsic limitations in spatial resolution and in retrieving North-South displacement components with InSAR, the results obtained from the Sentinel-1 stacking analysis alone cannot be conclusive. We have thus performed a DIC analysis by considering other remote sensing data, i.e., the DTMs obtained from airborne LiDAR surveys. This investigation is complementary to InSAR, as it provides information on displacements along the East-West and especially North-South directions. Considering the ground resolution of the available DTMs, the accuracy of the DIC analysis is expected to be on the order of ±0.1 m/a (Bickel et al., 2018), which is suitable to provide information in the specific case of Brienz, where the surface velocities are of m/a. The comparison between two selected sub-periods, i.e., 2015-2018 and 2018-2020, shows a clear increase in surface velocities mainly in the RB domain and towards the South. However, slight accelerations are also observed in the RD domain, especially in the westernmost portions at the elevations of the Brienz village. This is one of the areas where major damage is witnessed on the roads and infrastructures. Another area where we observe a slight increase in surface velocities is on the Southeast sectors towards the

Albula river. DIC approaches are a valid complementary method for the analysis of surface displacement components; however, datasets with suitable GSD are necessary to retrieve accurate measurements. The case of Brienz is rather unique, as it is unusual to have multi-temporal LiDAR surveys within 5 years. In the future, very high-resolution imagery available from new generation satellites (optical and SAR) with a spatial resolution on the order of 1 m will be an important additional source of information to be considered in such investigations.

We have combined the results of DInSAR stacking and the DIC analysis to reconstruct a full, 3-D picture of the surface deformation affecting the Brienz landslide complex. The combination of multiple Sentinel-1 orbits and DIC results has provided important information on the spatial distribution of the surface deformation. This approach allowed us to retrieve a more accurate representation of the displacement field and improved the agreement with the GNSS measurements. The surface deformation is characterized by a "patchy" pattern, which is representative of internal landslide compartments. This is in agreement with detailed evaluations of the 3-D displacements performed for the RB area and based on high resolution terrestrial LiDAR datasets (Kenner et al. 2022). The most relevant observations on the 3-D surface velocities are related to the upper reaches of the RB domain (i.e., North of GNSS station 6001), where the surface velocities have substantially increased during the period 2018-2020 compared with 2015-2018. The obtained 3-D results show that intrinsic limitations associated with phase aliasing can be only partially overcome. In the North-South direction, where the displacements are of several m/a, we could retrieve a better agreement between with the GNSS measurements. This is because the DIC analysis provides a good complement to the InSAR measurements. East-West components, however, are smaller in amplitude and thus suffer of accuracy problems also with DIC. On the other end, up-down components are exclusively measured through InSAR and cannot be mitigated with this analysis. Higher resolution datasets or constellation of satellite SAR sensors with more frequent acquisitions can help in retrieving a better representation of the 3-D behavior and allow for a more detailed kinematic interpretation of landslides based on the analysis of the displacement vector orientations (Kenner et al. 2022).

Among the discussed limitations, we note that a substantial underestimation of the landslide acceleration can occur if only spaceborne C-Band (i.e., currently Sentinel-1) interferometry is applied. Indeed, phase decorrelation might affect the spatial sampling of measurement points, while phase aliasing can cause large deviations from the correct velocity values. This has to be sensibly considered in systematic monitoring programs aimed at identifying surface displacement anomalies (Dehls et al. 2019; Crosetto et al. 2020; Bianchini et al. 2021). The parameters determining the accuracy of the results when using spaceborne and aerial imagery are the spatial and temporal resolution, as well as their intrinsic detection thresholds. This seems to be a trivial concept; however, it is not always carefully considered, and interpretations can be misleading. The amount of information available at the Brienz site is exceptional, and only in few alpine sites remote sensing investigations can be complemented with detailed surface geology and structural data, and/or validated with in-situ measurements. Especially in inaccessible regions, where remote sensing is often the only available data source to define active landslide domains and possibly build evolutionary scenarios and/or hazard assessments, we suggest a cautious evaluation of the InSAR results obtained with C-Band sensors only.

7. Authors' Responsibilities

AM and SL conceived the study. NJ performed the Sentinel-1 InSAR and stacking processing. AM performed the IPTA analysis, DIC, 3-D combination, and the validation with GNSS. TS performed the processing of Radarsat-2 and ALOS-2 PALSAR-2 interferometry. RC and UW performed the pre-processing of the Sentinel-1 datasets. AM, NJ and SL interpreted the results. AM and NJ wrote the paper. All co-authors revised the manuscript.

8. Declaration of Interest

The authors declare no conflict of interest.

9. Acknowledgements

We acknowledge the support of the Swiss Federal Office of Environment (Hugo Raetzo) providing access to ERS, Envisat ASAR, and Radarsat datasets. In-situ measurements are courtesy of the company CSD (https://www.csd.ch/, Valentin Gischig, Stefan Schneider). We thank Reto Thöni, Thomas Breitenmoser, and Daniel Figi from the company BTG (https://www.btgeo.ch/) for early discussions on the geology, surface displacement and evolution of the Brienz landslide.

10. Funding

Funding for this project was provided through a research agreement between ETH, AWN and the Gemeinde Albula/Alvra. The activities of GAMMA Remote Sensing were supported by the EU-RAMON project. ALOS-2 Data were acquired through the project EO-RA3, PI No.: ER3A2N534.

11. References

Aaron J, Loew S, Forrer M (2021) Recharge response and kinematics of an unusual earthflow in Liechtenstein. Landslides. https://doi.org/10.1007/s10346-021-01633-5

Agliardi F, Scuderi MM, Fusi N, Collettini C (2020) Slow-to-fast transition of giant creeping rockslides modulated by undrained loading in basal shear zones. Nat Commun 11:1–11. https://doi.org/10.1038/s41467-020-15093-3

Aoki Y, Furuya M, De Zan F, et al (2021) L-band Synthetic Aperture Radar: Current and future applications to Earth sciences. Earth, Planets and Space 73:56. https://doi.org/10.1186/s40623-021-01363-x

Berardino P, Fornaro G, Lanari R, Sansosti E (2002) A new algorithm for surface deformation monitoring based on small baseline differential SAR interferograms. IEEE Transactions on Geoscience and Remote Sensing 40:2375–2383. https://doi.org/10.1109/TGRS.2002.803792

Bianchini S, Solari L, Bertolo D, et al (2021) Integration of Satellite Interferometric Data in Civil Protection Strategies for Landslide Studies at a Regional Scale. Remote Sensing 13:1881. https://doi.org/10.3390/rs13101881

Bickel VT, Manconi A, Amann F (2018) Quantitative Assessment of Digital Image Correlation Methods to Detect and Monitor Surface Displacements of Large Slope Instabilities. Remote Sensing 10:865. https://doi.org/10.3390/rs10060865

Bontemps N, Lacroix P, Doin M-P (2018) Inversion of deformation fields time-series from optical images, and application to the long term kinematics of slow-moving landslides in Peru. Remote Sensing of Environment 210:144–158. https://doi.org/10.1016/j.rse.2018.02.023

Bürgmann R, Rosen PA, Fielding EJ (2000) Synthetic aperture radar interferometry to measure Earth’s surface topography and its deformation. Annual Review of Earth and Planetary Sciences 28:169–209

Casagli N, Cigna F, Bianchini S, et al (2016) Landslide mapping and monitoring by using radar and optical remote sensing: Examples from the EC-FP7 project SAFER. Remote Sensing Applications: Society and Environment 4:92–108. https://doi.org/10.1016/j.rsase.2016.07.001

Casu F, Manconi A (2016) Four-dimensional surface evolution of active rifting from spaceborne SAR data. Geosphere GES01225.1. https://doi.org/10.1130/GES01225.1

Casu F, Manconi A, Pepe A, Lanari R (2011) Deformation Time-Series Generation in Areas Characterized by Large Displacement Dynamics: The SAR Amplitude Pixel-Offset SBAS Technique. IEEE Transactions on Geoscience and Remote Sensing 49:2752–2763. https://doi.org/10.1109/TGRS.2010.2104325

Cigna F, Bateson LB, Jordan CJ, Dashwood C (2014) Simulating SAR geometric distortions and predicting Persistent Scatterer densities for ERS-1/2 and ENVISAT C-band SAR and InSAR applications: Nationwide feasibility assessment to monitor the landmass of Great Britain with SAR imagery. Remote Sensing of Environment 152:441–466. https://doi.org/10.1016/j.rse.2014.06.025

Ciuffi P, Bayer B, Berti M, et al (2021) Deformation Detection in Cyclic Landslides Prior to Their Reactivation Using Two-Pass Satellite Interferometry. Applied Sciences 11:3156. https://doi.org/10.3390/app11073156

Costantini M (1998) A novel phase unwrapping method based on network programming. IEEE Transactions on Geoscience and Remote Sensing 36:813–821. https://doi.org/10.1109/36.673674

Crippa C, Franzosi F, Zonca M, et al (2020) Unraveling Spatial and Temporal Heterogeneities of Very Slow Rock-Slope Deformations with Targeted DInSAR Analyses. Remote Sensing 12:1329. https://doi.org/10.3390/rs12081329

Crosetto M, Monserrat O, Cuevas-González M, et al (2016) Persistent Scatterer Interferometry: A review. ISPRS Journal of Photogrammetry and Remote Sensing 115:78–89. https://doi.org/10.1016/j.isprsjprs.2015.10.011

Crosetto M, Solari L, Mróz M, et al (2020) The Evolution of Wide-Area DInSAR: From Regional and National Services to the European Ground Motion Service. Remote Sensing 12:2043. https://doi.org/10.3390/rs12122043

Dehls JF, Larsen Y, Marinkovic P, et al (2019) INSAR.No: A National Insar Deformation Mapping/Monitoring Service In Norway – From Concept To Operations. In: IGARSS 2019 - 2019 IEEE International Geoscience and Remote Sensing Symposium. pp 5461–5464

Delbridge BG, Bürgmann R, Fielding E, et al (2016) Three-dimensional surface deformation derived from airborne interferometric UAVSAR: Application to the Slumgullion Landslide. J Geophys Res Solid Earth 121:2015JB012559. https://doi.org/10.1002/2015JB012559

Dini B, Daout S, Manconi A, Loew S (2019) Classification of slope processes based on multitemporal DInSAR analyses in the Himalaya of NW Bhutan. Remote Sensing of Environment 233:111408. https://doi.org/10.1016/j.rse.2019.111408

Ebmeier SK, Andrews BJ, Araya MC, et al (2018) Synthesis of global satellite observations of magmatic and volcanic deformation: implications for volcano monitoring & the lateral extent of magmatic domains. J Appl Volcanol 7:2. https://doi.org/10.1186/s13617-018-0071-3

Elefante S, Manconi A, Bonano M, et al (2014) Three-dimensional ground displacements retrieved from SAR data in a landslide emergency scenario. In: Geoscience and Remote Sensing Symposium (IGARSS), 2014 IEEE International. pp 2400–2403

Ferretti A, Fumagalli A, Novali F, et al (2011) A New Algorithm for Processing Interferometric Data-Stacks: SqueeSAR. IEEE Transactions on Geoscience and Remote Sensing 49:3460–3470. https://doi.org/10.1109/TGRS.2011.2124465

Ferretti A, Prati C, Rocca F (2001) Permanent scatterers in SAR interferometry. IEEE Transactions on Geoscience and Remote Sensing 39:8–20. https://doi.org/10.1109/36.898661

Fey C, Rutzinger M, Wichmann V, et al (2015) Deriving 3D displacement vectors from multi-temporal airborne laser scanning data for landslide activity analyses. GIScience & Remote Sensing 52:437–461. https://doi.org/10.1080/15481603.2015.1045278

Figi D, Thöny R, Breitenmoser T, et al (2022) Rutschung Brienz/Brinzauls (GR): Geologisch-kinematisches und hydrogeologisches Modell. 27/2:1–34

Frattini P, Crosta GB, Rossini M, Allievi J (2018) Activity and kinematic behaviour of deep-seated landslides from PS-InSAR displacement rate measurements. Landslides 15:1053–1070. https://doi.org/10.1007/s10346-017-0940-6

Glueer F, Loew S, Manconi A, Aaron J (2019) From Toppling to Sliding: Progressive Evolution of the Moosfluh Landslide, Switzerland. Journal of Geophysical Research: Earth Surface 124:2899–2919. https://doi.org/10.1029/2019JF005019

Gorelick N, Hancher M, Dixon M, et al (2017) Google Earth Engine: Planetary-scale geospatial analysis for everyone. Remote Sensing of Environment. https://doi.org/10.1016/j.rse.2017.06.031

Häusler M, Gischig V, Thöny R, et al (2022) Monitoring the changing seismic site response of a fast-moving rockslide (Brienz/Brinzauls, Switzerland). Geophysical Journal International 229:299–310. https://doi.org/10.1093/gji/ggab473

Hooper A (2008) A multi-temporal InSAR method incorporating both persistent scatterer and small baseline approaches. Geophys Res Lett 35:L16302. https://doi.org/10.1029/2008GL034654

Jelének J, Kopačková-Strnadová V (2021) Synergic use of Sentinel-1 and Sentinel-2 data for automatic detection of earthquake-triggered landscape changes: A case study of the 2016 Kaikoura earthquake (Mw 7.8), New Zealand. Remote Sensing of Environment 265:112634. https://doi.org/10.1016/j.rse.2021.112634

Kääb A, Strozzi T, Werner C (2009) An overview of fast-flowing glaciers on Svalbard from satellite SAR speckle tracking and matching of repeat optical images. EGUGA 11834

Kenner R, Gischig V, Gojcic Z, et al (2022) The potential of point clouds for the analysis of rock kinematics in large slope instabilities: examples from the Swiss Alps: Brinzauls, Pizzo Cengalo and Spitze Stei. Landslides. https://doi.org/10.1007/s10346-022-01852-4

Lanari R, Bonano M, Casu F, et al (2020) Automatic Generation of Sentinel-1 Continental Scale DInSAR Deformation Time Series through an Extended P-SBAS Processing Pipeline in a Cloud Computing Environment. Remote Sensing 12:2961. https://doi.org/10.3390/rs12182961

Li M, Zhang L, Shi X, et al (2019) Monitoring active motion of the Guobu landslide near the Laxiwa Hydropower Station in China by time-series point-like targets offset tracking. Remote Sensing of Environment 221:80–93. https://doi.org/10.1016/j.rse.2018.11.006

Lissak C, Bartsch A, De Michele M, et al (2020) Remote Sensing for Assessing Landslides and Associated Hazards. Surv Geophys. https://doi.org/10.1007/s10712-020-09609-1

Lundgren P, Usai S, Sansosti E, et al (2001) Modeling surface deformation observed with synthetic aperture radar interferometry at Campi Flegrei caldera. Journal of Geophysical Research: Solid Earth 106:19355–19366. https://doi.org/10.1029/2001JB000194

Manconi A (2021) How phase aliasing limits systematic space-borne DInSAR monitoring and failure forecast of alpine landslides. Engineering Geology 287:106094. https://doi.org/10.1016/j.enggeo.2021.106094

Manconi A, Casu F, Ardizzone F, et al (2014) Brief communication: Rapid mapping of event landslides: the 3 December 2013 Montescaglioso landslide (Italy). Natural Hazards and Earth System Sciences Discussions 2:1465–1479

Manconi A, Kourkouli P, Caduff R, et al (2018) Monitoring Surface Deformation over a Failing Rock Slope with the ESA Sentinels: Insights from Moosfluh Instability, Swiss Alps. Remote Sensing 10:672. https://doi.org/10.3390/rs10050672

Manzo M, Ricciardi GP, Casu F, et al (2006) Surface deformation analysis in the Ischia Island (Italy) based on spaceborne radar interferometry. Journal of Volcanology and Geothermal Research 151:399–416. https://doi.org/10.1016/j.jvolgeores.2005.09.010

Peng M, Lu Z, Zhao C, et al (2022) Mapping land subsidence and aquifer system properties of the Willcox Basin, Arizona, from InSAR observations and independent component analysis. Remote Sensing of Environment 271:112894. https://doi.org/10.1016/j.rse.2022.112894

Petley D (2023) Summary of the 15 June 2023 Brienz/Brinzauls rockslide collapse in the Swiss Alps. In: The Landslide Blog. https://blogs.agu.org/landslideblog/2023/06/21/brienz-brinzauls-rockslide/. Accessed 10 Sep 2023

Raetzo H, Wegmüller U, Strozzi T, et al (2007) Monitoring of Lumnez Landslide with ERS and ENVISAT SAR data. In: Proceedings of Envisat Symposium, Montreux, Switzerland, ESA SP-636

Raspini F, Bianchini S, Ciampalini A, et al (2019) Persistent Scatterers continuous streaming for landslide monitoring and mapping: the case of the Tuscany region (Italy). Landslides. https://doi.org/10.1007/s10346-019-01249-w

Rosen P, Hensley S, Shaffer S, et al (2017) The NASA-ISRO SAR (NISAR) mission dual-band radar instrument preliminary design. In: 2017 IEEE International Geoscience and Remote Sensing Symposium (IGARSS). pp 3832–3835

Schneider M, Oestreicher N, Loew S (2023) Rockfall monitoring with a Doppler radar on an active rock slide complex in Brienz/Brinzauls (Switzerland). EGUsphere 1–25. https://doi.org/10.5194/egusphere-2023-555

Singleton A, Li Z, Hoey T, Muller J-P (2014) Evaluating sub-pixel offset techniques as an alternative to D-InSAR for monitoring episodic landslide movements in vegetated terrain. Remote Sensing of Environment 147:133–144. https://doi.org/10.1016/j.rse.2014.03.003

Stead D, Eberhardt E (2013) Understanding the Mechanics of Large Landslides. Italian Journal of Engineering Geology and Environment 85–112. https://doi.org/10.4408/IJEGE.2013-06.B-07

Storni E, Hugentobler M, Manconi A, Loew S (2020) Monitoring and analysis of active rockslide-glacier interactions (Moosfluh, Switzerland). Geomorphology 371:107414. https://doi.org/10.1016/j.geomorph.2020.107414

Strozzi T, Luckman A, Murray T, et al (2002) Glacier motion estimation using SAR offset-tracking procedures. IEEE Transactions on Geoscience and Remote Sensing 40:2384–2391

Stumpf A, Malet J-P, Delacourt C (2017) Correlation of satellite image time-series for the detection and monitoring of slow-moving landslides. Remote Sensing of Environment 189:40–55. https://doi.org/10.1016/j.rse.2016.11.007

Tomás R, Li Z (2017) Earth Observations for Geohazards: Present and Future Challenges. Remote Sensing 9:194. https://doi.org/10.3390/rs9030194

Torres R, Snoeij P, Geudtner D, et al (2012) GMES Sentinel-1 mission. Remote Sensing of Environment 120:9–24. https://doi.org/10.1016/j.rse.2011.05.028

Wasowski J, Bovenga F (2014) Investigating landslides and unstable slopes with satellite Multi Temporal Interferometry: Current issues and future perspectives. Engineering Geology 174:103–138. https://doi.org/10.1016/j.enggeo.2014.03.003

Wegmüller U, Werner C, Strozzi T, et al (2016) Sentinel-1 support in the GAMMA software. Procedia Computer Science 100:1305–1312

Werner C, Wegmuller U, Strozzi T, Wiesmann A (2003) Interferometric point target analysis for deformation mapping. In: IGARSS 2003. 2003 IEEE International Geoscience and Remote Sensing Symposium. Proceedings (IEEE Cat. No.03CH37477). pp 4362–4364 vol.7

Zinno I, Bonano M, Buonanno S, et al (2018) National Scale Surface Deformation Time Series Generation through Advanced DInSAR Processing of Sentinel-1 Data within a Cloud Computing Environment. IEEE Transactions on Big Data 1–1. https://doi.org/10.1109/TBDATA.2018.2863558

Supplementary Information

Table S1. Coordinates (in Coordinate System CH1903/LV03, EPSG 21781) of the GNSS points reported in Figure 2. The reported date is referred to the last measurement considered in this work.

GNSS Point	X Coordinate	Y Coordinate	Z Coordinate	Last measurement (DD.MM.YY)
11	764635.52	171058.8	1165.95	18.08.20
12	764630.68	170634.28	1073.81	18.08.20
13	764680.33	170430.26	1021.68	18.08.20
14	764693.69	169952.06	898.11	18.08.20
15	764527.54	169863.47	872.9	18.08.20
22	765034.81	170380.71	1004.44	18.08.20
23	765120.08	169995.9	904.92	18.08.20
31	765230.36	171434.87	1331.13	28.05.18
32	765459.98	170910.46	1112.86	18.08.20
33	765553.79	170571.24	1008.5	18.08.20
34	765672.72	170285.44	923.04	23.05.13
35	765794.15	170077.26	885.04	18.08.20
41	763874.68	170972.07	1125.15	14.06.19
42	764131.97	170843.6	1134.77	14.06.19
114	764704.98	169987.35	907.16	18.08.20
115	764523.38	169862.71	872.64	18.08.20
122	765057.1	170386.28	1003.55	18.08.20
123	765122.15	169997.69	905.09	14.06.19
131	765316.51	171464.36	1346.68	28.05.18
134	765674.22	170284.59	922.8	18.08.20
1001	764654.03	171653.21	1573.18	11.05.20
1002	764657.92	171741.34	1602.53	11.05.20
1003	764650.44	171819.48	1644.93	11.05.20
1004	764690.84	171848.46	1669.81	29.03.19
1005	764774.18	171868.76	1697.39	11.05.20
1006	764808.18	171882.92	1713.96	24.05.17
1007	764806.59	171975.58	1752.97	11.05.20
1008	764798.25	171978.35	1755.04	11.05.20
1009	764788.01	171967.76	1753.23	11.05.20
1010	764831.6	172072.77	1790.05	11.05.20
1011	764845.87	172164.24	1796.07	14.06.19
1012	764742.94	172199.98	1813.08	14.06.19
1013	764817.08	172329.05	1791.34	14.06.19
1014	765145.54	172294.12	1760.12	14.06.19
1015	765280.08	172039.36	1694.16	14.06.19
1016	764598.13	171537.24	1487.05	11.05.20
1017	764595.99	171540.78	1487.56	03.11.17
2001	764695.8	171899.54	1701.93	11.05.20
2002	764712.44	171972.57	1734.2	11.05.20
2003	764723.83	172073.76	1776.56	11.05.20
2004	764706.81	172123.57	1803.5	11.05.20

2005	764849.87	172025.3	1765.08	11.05.20
2006	764947.99	171954.64	1712.27	11.05.20
2007	764960.2	171994.39	1741.12	11.05.20
2008	764939.27	172050.1	1763.04	11.05.20
3001	764122.73	171726.65	1438.6	14.06.19
3002	764078.37	171292.87	1285.96	14.06.19
3003	763830.86	171329.31	1222.76	14.06.19
3004	764358.14	170368.38	1004.29	14.06.19
3005	765407.69	171035.03	1162.84	11.05.20
3006	765597.03	171193.68	1214.38	14.06.19
3007	765636.04	171401.77	1369.73	14.06.19
3008	765879.13	171825.06	1484.39	14.06.19
3009	765802.9	171946.3	1537.51	14.06.19
3010	765991.29	172043.78	1539.14	14.06.19
3011	765479.64	172117.39	1646.6	14.06.19
3012	765687.8	172298.1	1717.9	14.06.19
3013	765100.9	172559.88	1861.83	14.06.19
3014	764612.36	172563.9	1881.27	14.06.19
3015	764559.12	172269.29	1763.02	14.06.19
3020	764556.48	170753.96	1114.53	18.08.20
3021	764357.72	171051.89	1200.88	18.08.20
3022	764276.44	170954.53	1187.21	18.08.20
3023	764295.98	171308.81	1304.29	18.08.20
3024	764329.59	171318.34	1309.42	18.08.20
5001	764993.2	170891.21	1157.19	04.11.20
5002	764793.98	170585.19	1064.86	04.11.20
5003	765476.83	170674.25	1054.6	04.11.20
6001	764518.48	171419.19	1378.04	04.11.20
6002	764649.29	171819.72	1644.96	04.11.20
6003	764797.02	171968.55	1753.15	04.11.20
6004	764866.93	171970.95	1738.31	04.11.20
6005	764702.34	171888.14	1698.95	04.11.20
6006	764703.79	171977.2	1736.68	04.11.20
7001	764422.86	171221.12	1286.39	04.11.20
7002	764447.31	170892.64	1156.6	04.11.20
12160151	763927.61	170397.7	1012.92	14.06.19
12160218	765443.67	172557.38	1851.03	14.06.19
12160224	764120.6	171722.74	1438.87	14.06.19
12160229	765889.63	170914.1	1093.29	14.06.19
12160230	765035.5	170709.18	1127.26	18.08.20
12160235	764594.81	170121.85	940.21	18.08.20

Table S2. Summary table of the parameters used for the Digital Image Correlation analysis. Additional information on the parameters and their effect on the results can be found in Bickel et al., 2018.

Parameter	Value
Template window (pixels)	128x128
skip (pixels)	16
Oversampling factor	2

Figure S1. Selected interferograms for the ERS1/2 and Envisat ASAR satellite imagery, ascending orbit. The results are strongly affected by phase decorrelation and do not allow us to identify whether surface deformation was already present over the Brienz landslide complex during the period 1992-2010.

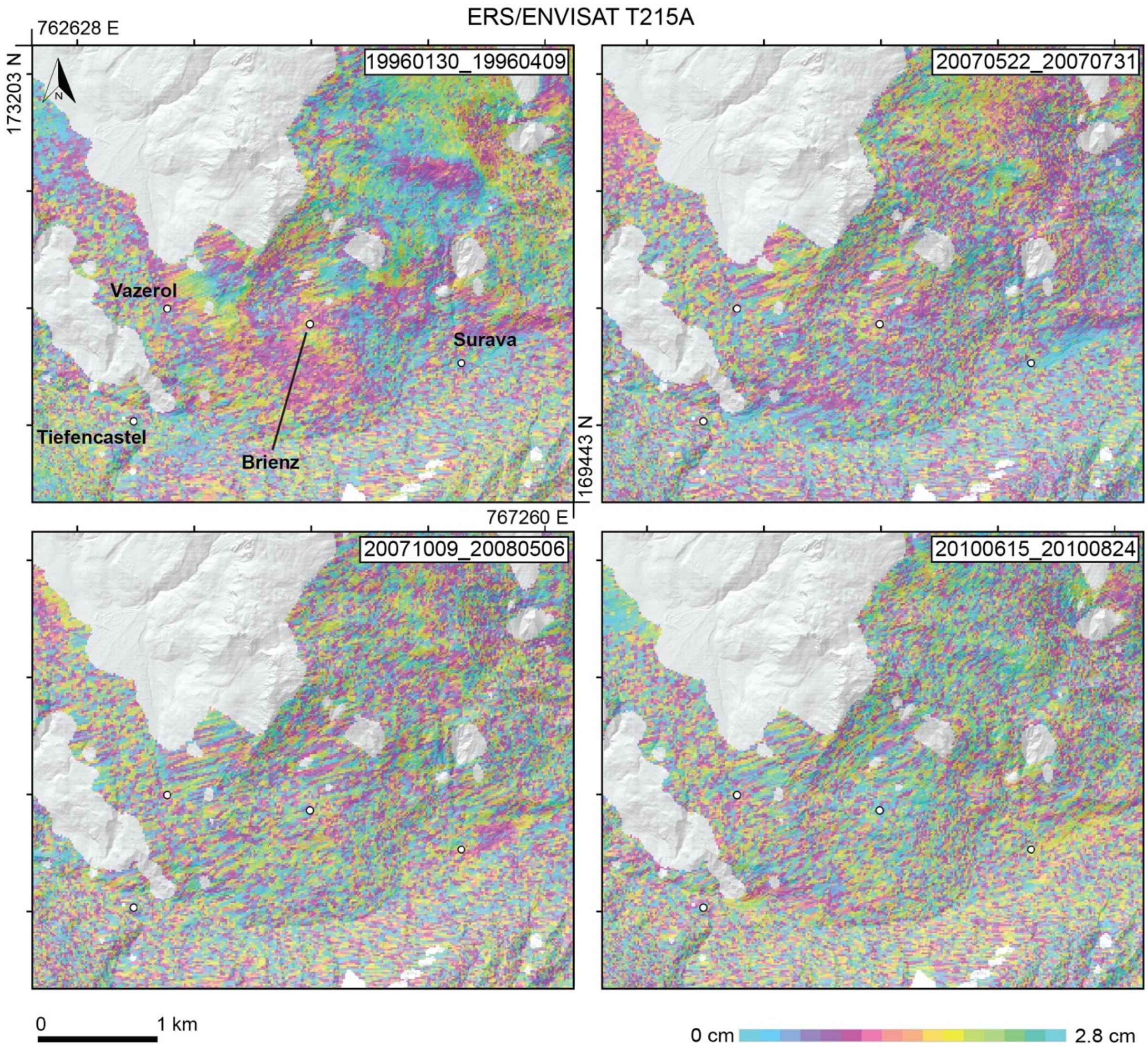

Figure S2. Selected interferograms for the ERS1/2 and Envisat ASAR satellite imagery, descending orbit. The results are strongly affected by phase decorrelation and do not allow us to identify whether surface deformation was already present over the Brienz landslide complex during the period 1992-2010.

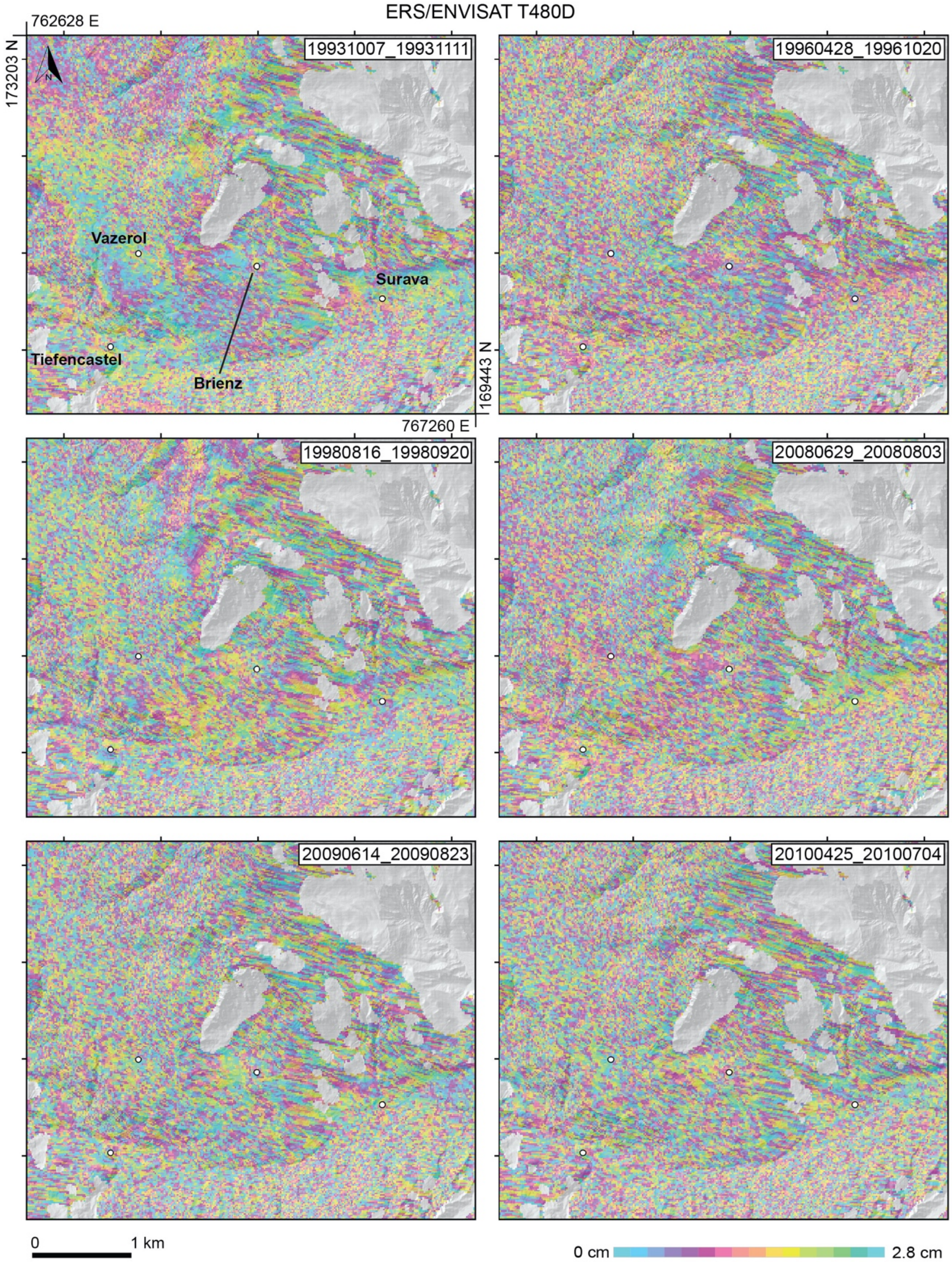

Figure S3. Selected interferograms for the Radarsat-2 satellite imagery, ascending orbit. The results are strongly affected by phase decorrelation.

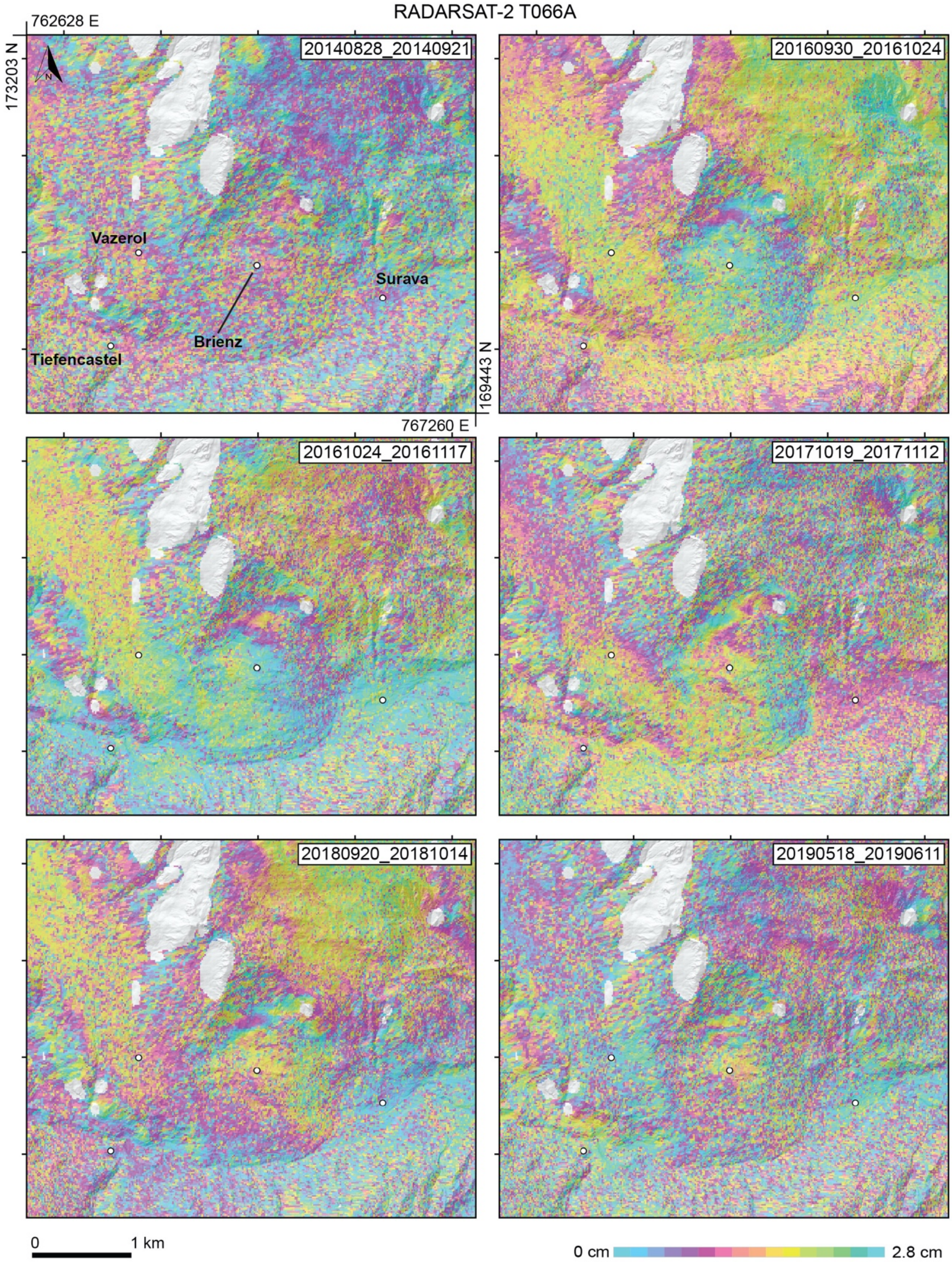

Figure S4. Selected interferograms for the Radarsat-2 satellite imagery, descending orbit. The results are strongly affected by phase decorrelation, however some interferograms show deformation over RB and RD.

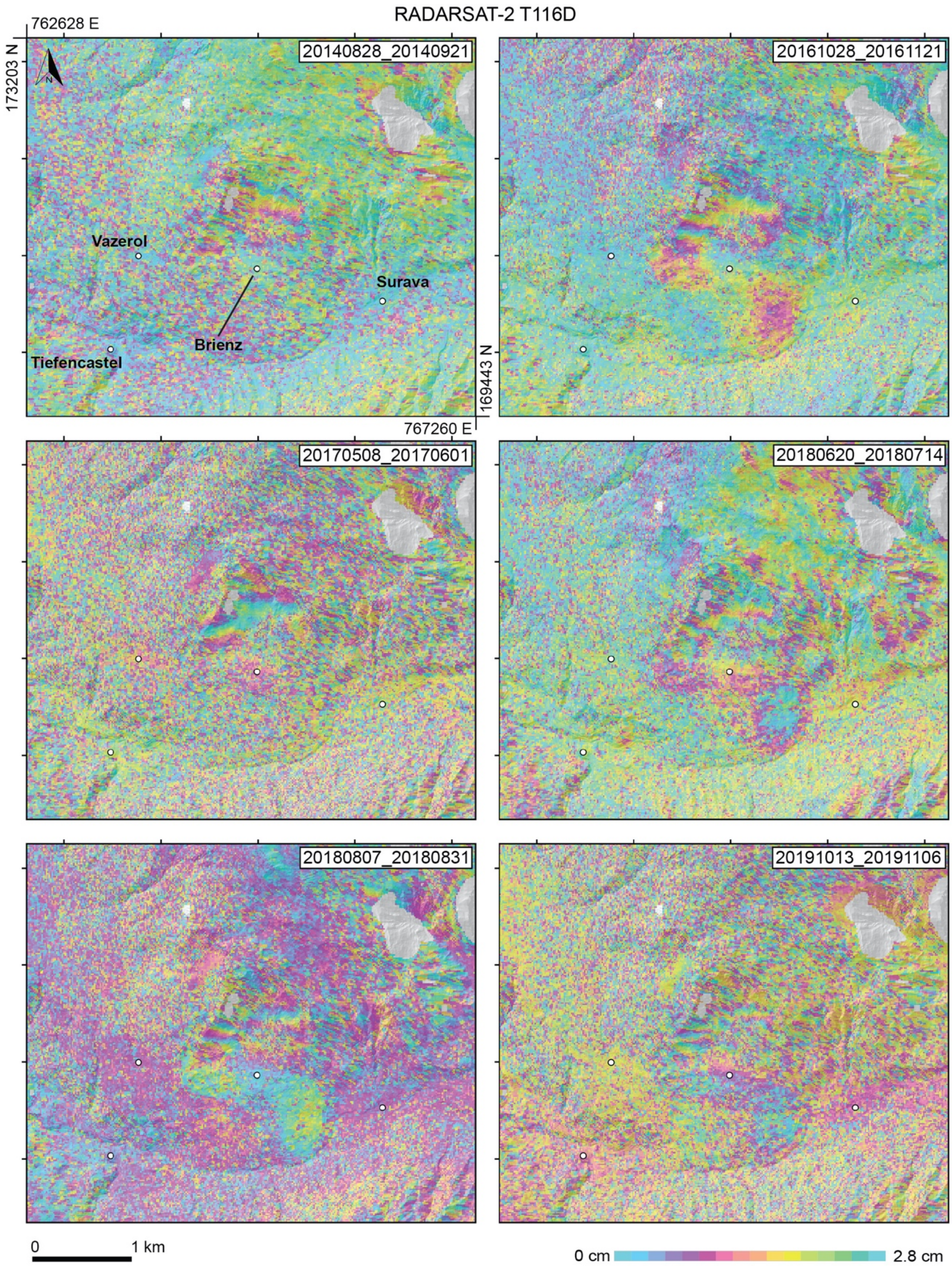

Figure S5. Selected interferograms for the Sentinel-1 satellite imagery, ascending orbit T015.

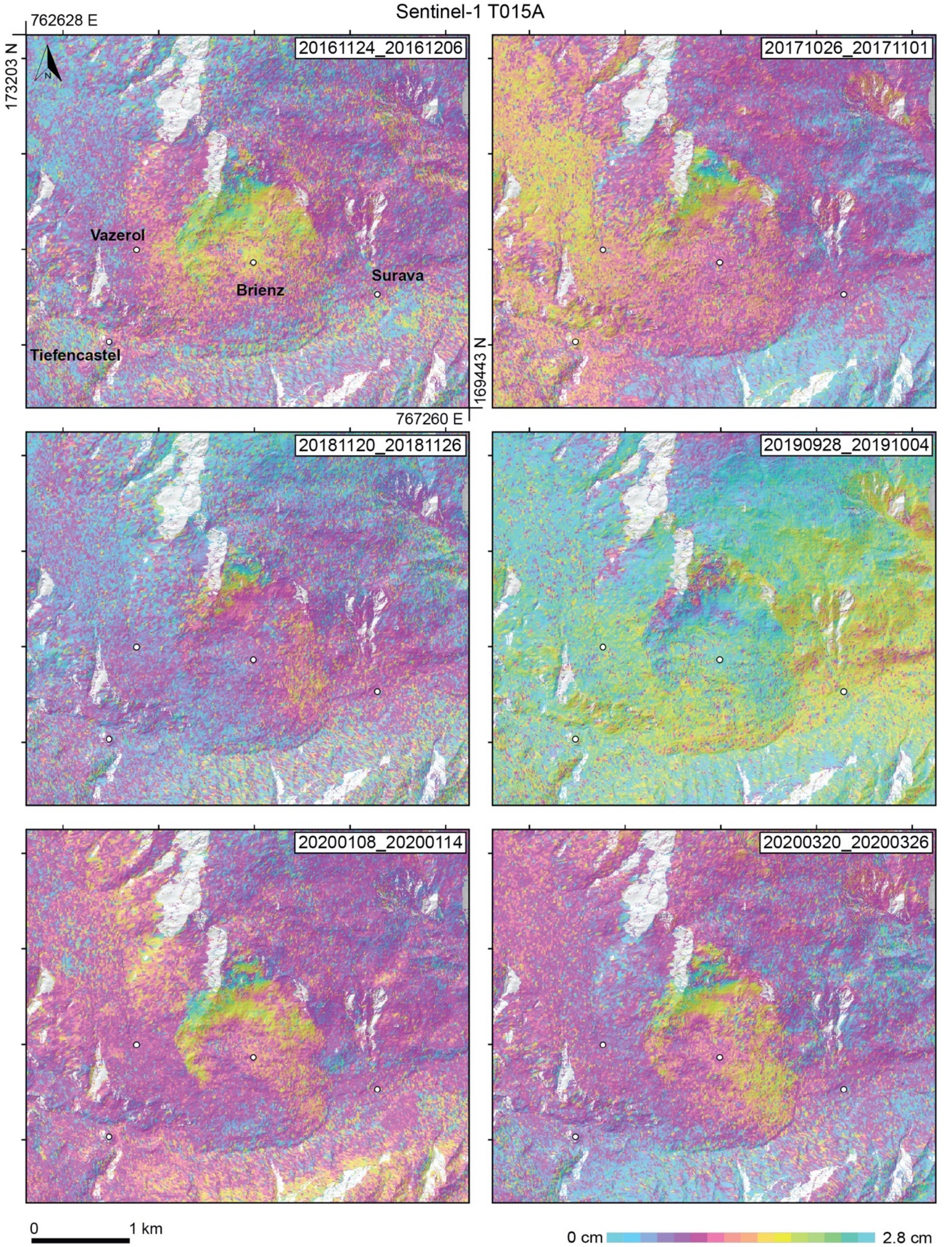

Figure S6. Selected interferograms for the Sentinel-1 satellite imagery, descending orbit T066.

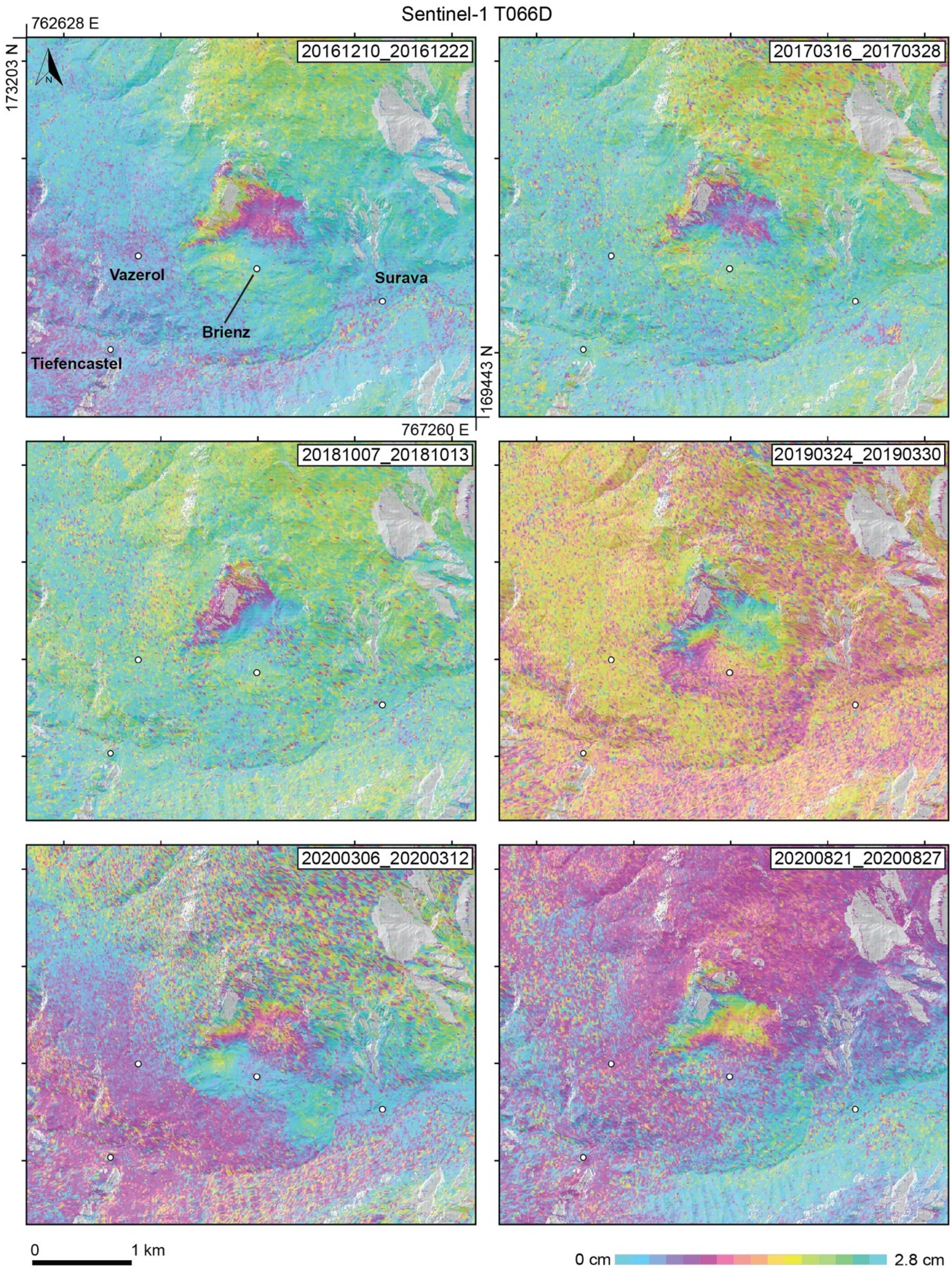

Figure S7. Selected interferograms for the Sentinel-1 satellite imagery, descending orbit T168.

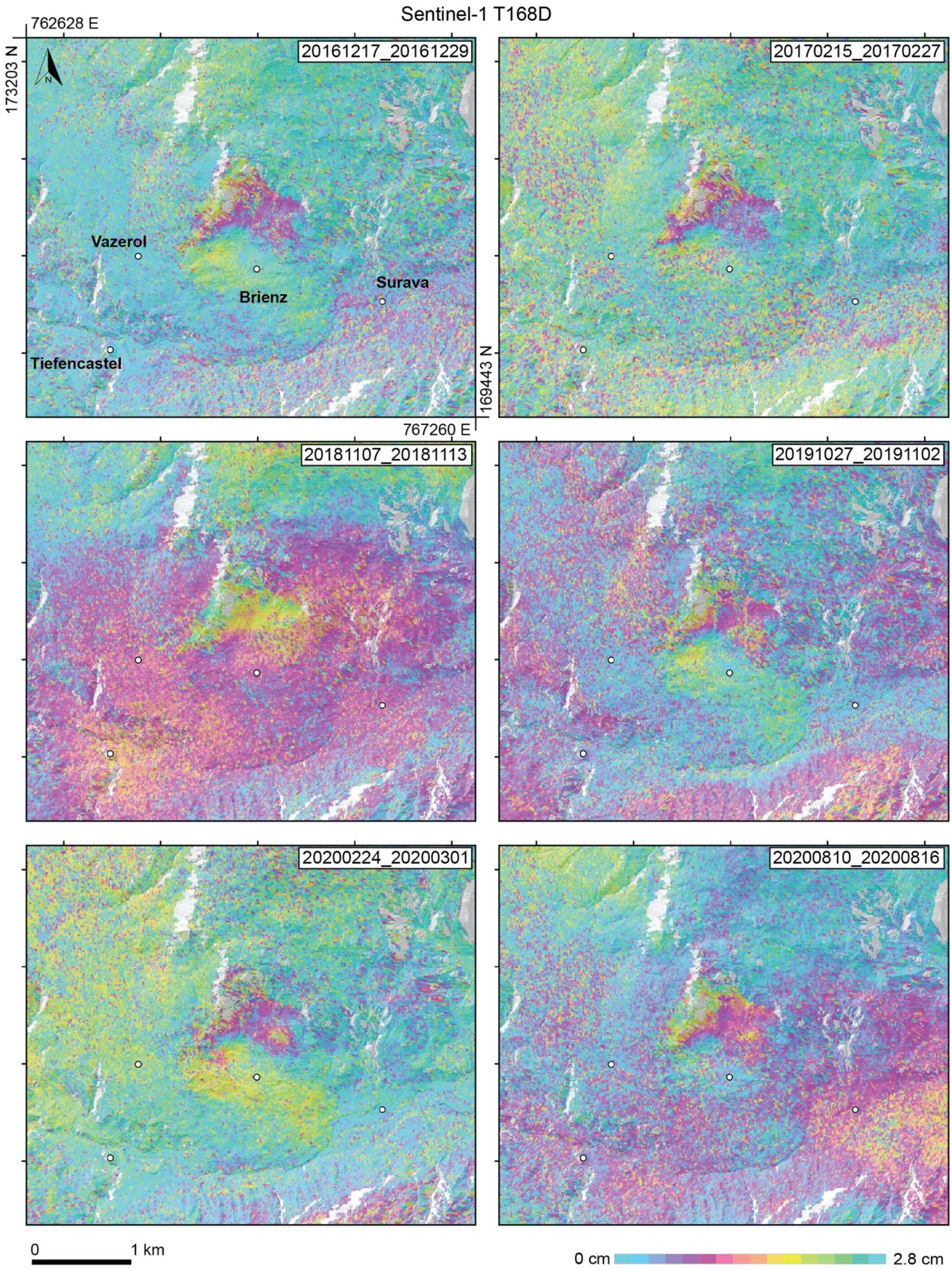

Figure S8. Selected ALOS PALSAR-2 L-band interferograms, descending orbit. (top) Comparison between 14-days interferogram in L-band and 6-days interferogram in C-band. (bottom) Comparison between 14-days and 3-months interferograms with L-band, detail over RB and IL.

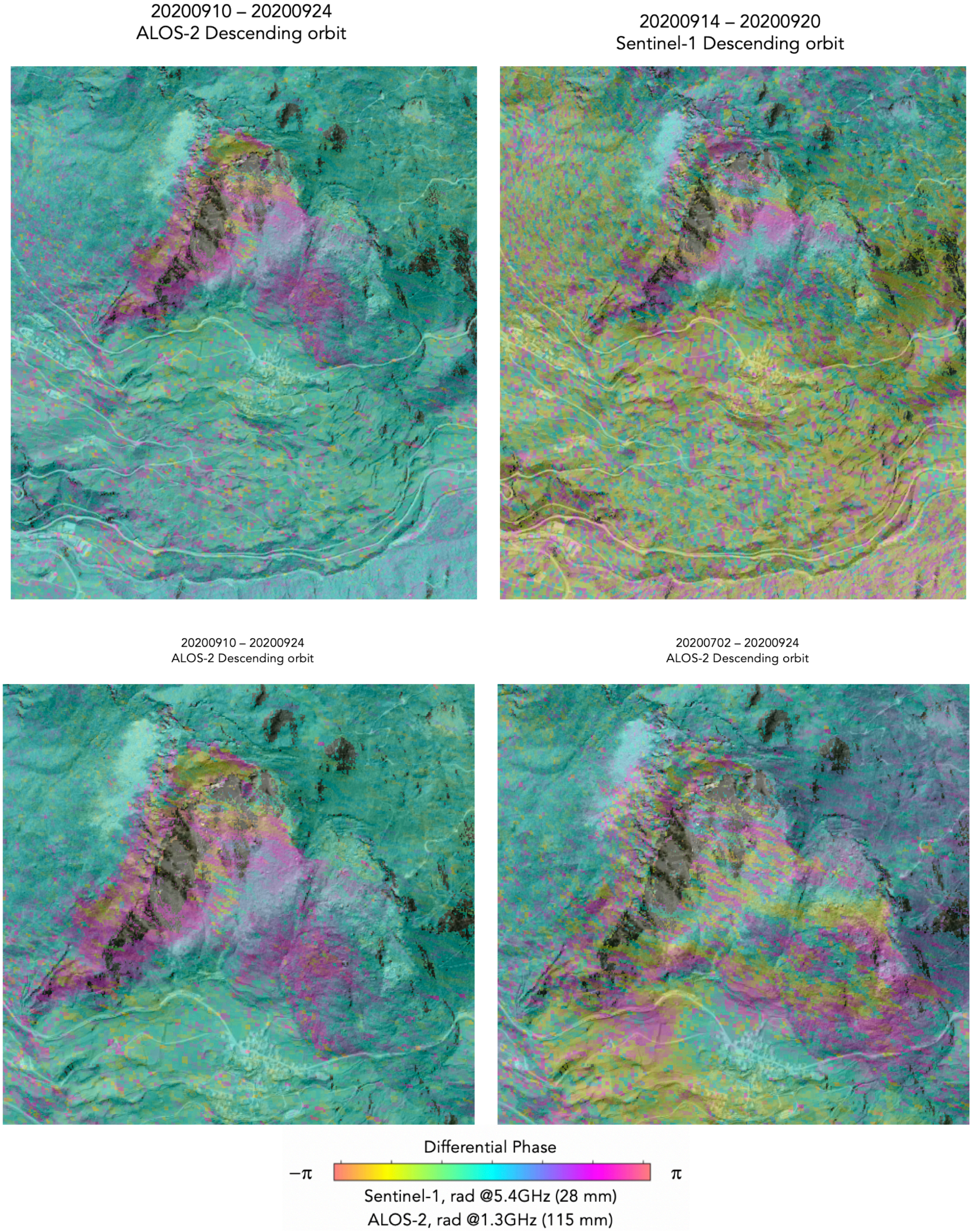

Figure S9. Selected Sentinel-1 ascending (top) and descending (bottom) displacement time series results for a point located in the Brienz village. Displacements are in the satellite LOS. The opposite displacement directions, i.e., away from satellite in ascending orbit and towards the satellite in descending orbit, denotes a strong horizontal component of the deformation field.

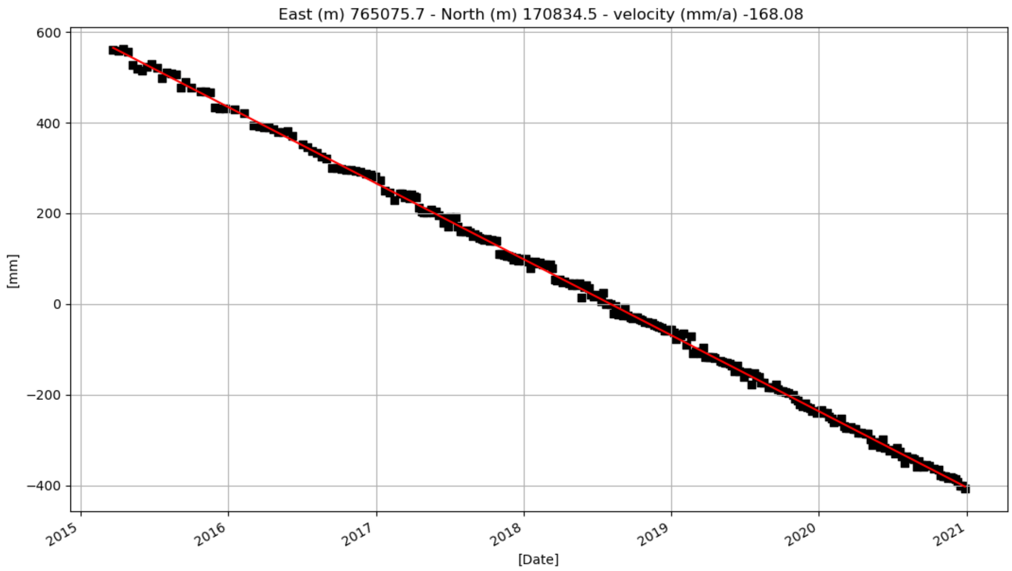

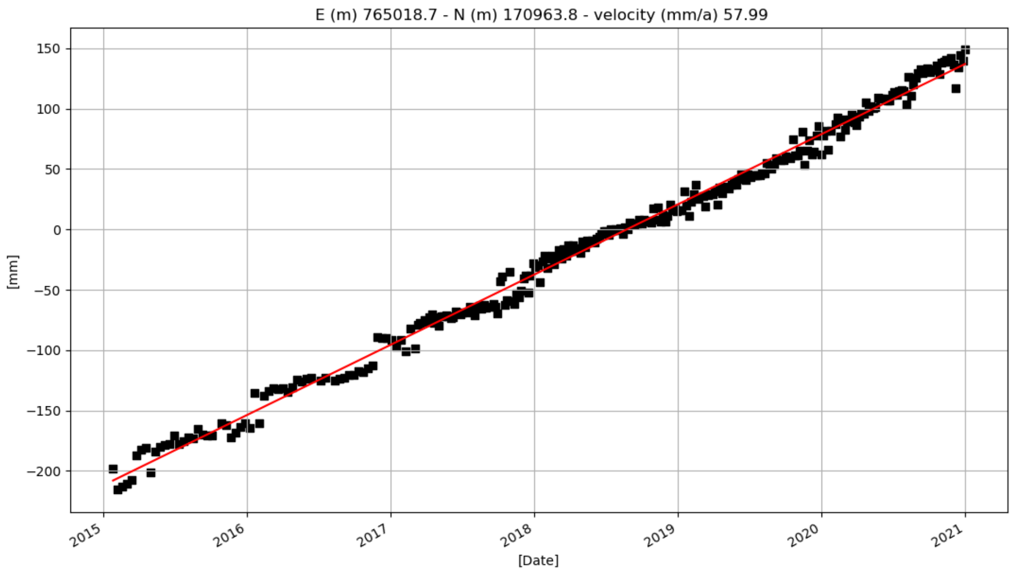

Figure S10. (top) DIC results for the East-West direction (unfiltered). The largest surface velocities are in the RD domain. In some areas, a slight increase is noted in the 2018-2020 period compared to 2015-2018. Some local artefacts are visible in the results due to rock fall activity (black circles). (bottom) DIC results for the North-South direction (unfiltered). The largest surface velocities are in the RB domain. There, a remarkable increase is noted in the 2018-2020 period compared to 2015-2018. Some local artefacts are visible in the results due to rock fall activity (black circles) and road maintenance (black rectangle).